NIH Public Access
Author Manuscript
Behav Brain Res. Author manuscript; available in PMC 2014 October 01.

Published in final edited form as:
Behav Brain Res. 2013 October 1; 254: 50–64. doi:10.1016/j.bbr.2013.07.005.

HIPPOCAMPAL AND SUBICULAR EFFERENTS AND AFFERENTS OF THE PERIRHINAL, POSTRHINAL, AND ENTORHINAL CORTICES OF THE RAT

Kara L. Agster[1] and **Rebecca D. Burwell**[1,2]

[1]Department of Neuroscience, Brown University, Providence, RI, 02912 USA

[2]Department of Cognitive, Linguistic, and Psychological Sciences, Brown University, Providence, RI, 02912 USA

Abstract

Available evidence suggests there is functional differentiation among hippocampal and parahippocampal subregions and along the dorsoventral (septotemporal) axis of the hippocampus. The aim of this study was to characterize and compare the efferent and afferent connections of perirhinal areas 35 and 36, postrhinal cortex, and the lateral and medial entorhinal areas (LEA and MEA) with dorsal and ventral components of the hippocampal formation (dentate gyrus, hippocampus cornu ammonis fields, and subiculum) as well as the presubiculum, and the parasubiculum. The entorhinal connections were also characterized with respect to the LEA and MEA dentate gyrus-projecting bands. In general, the entorhinal connections with the hippocampal formation are much stronger than the perirhinal and postrhinal connections. The entorhinal cortex projects strongly to all components of the hippocampal formation, whereas the perirhinal and postrhinal cortices project weakly and only to CA1 and the subiculum. In addition, the postrhinal cortex preferentially targets the dorsal CA1 and subiculum, whereas the perirhinal cortex targets ventral subiculum. Similarly, the perirhinal cortex receives more input from ventral hippocampal formation structures and the postrhinal cortex receives more input from dorsal hippocampal structures. The LEA and the MEA medial band are more strongly interconnected with ventral hippocampal structures, whereas the MEA lateral band is more interconnected with dorsal hippocampal structures. With regard to the presubiculum and parasubiculum, the postrhinal cortex and the MEA lateral band receive stronger input from the dorsal presubiculum and caudal parasubiculum. In contrast, the LEA and MEA medial bands receive stronger input from the ventral presubiculum and rostral parasubiculum.

© 2013 Elsevier B.V. All rights reserved.

Please direct correspondence and reprint requests to: Rebecca D. Burwell, Ph.D., Department of Cognitive, Linguistic, and Psychological Sciences, Brown University, 190 Thayer St., Providence, RI 02912 USA, phone: 011-1-401-863-9208, fax: 011-1-401-863-1300, Rebecca_Burwell@Brown.edu.
[1]Present address of KLA is 4200 Medical Biomolecular Research Building (MBRB), 111 Mason Farm Road, UNC-Chapel Hill, Chapel Hill, NC 27599.

Publisher's Disclaimer: This is a PDF file of an unedited manuscript that has been accepted for publication. As a service to our customers we are providing this early version of the manuscript. The manuscript will undergo copyediting, typesetting, and review of the resulting proof before it is published in its final citable form. Please note that during the production process errors may be discovered which could affect the content, and all legal disclaimers that apply to the journal pertain.

Conflict of interest
The authors declare no conflicts of interest.

NIH-PA Author Manuscript
NIH-PA Author Manuscript
NIH-PA Author Manuscript

NIH-PA Author Manuscript

NIH-PA Author Manuscript

NIH-PA Author Manuscript

Keywords

anterograde; retrograde; tract tracing; parahippocampal; Hippocampal formation; dentate gyrus; parahippocampal region

1. Introduction

The importance of the hippocampus to learning and memory was recognized with the ground breaking case of H.M. [1]. H.M.'s profound amnesia led to a preponderance of studies exploring the nature of hippocampal contributions to memory. Whereas early studies focused on the hippocampus itself, over time the field has expanded to include surrounding areas, now collectively termed the hippocampal system (Figure 1 and Figure 2A). According to one nomenclature, the hippocampal system includes the hippocampal formation and the parahippocampal region [2]. The hippocampal formation includes the dentate gyrus (DG), hippocampus proper (comprising fields CA3, CA2, and CA1), and the subiculum. The parahippocampal region includes the perirhinal (PER), postrhinal (POR), entorhinal, presubicular, and parasubicular cortices. Although some of these regions have received more attention in the literature than others, most experts now agree that structures beyond the hippocampus contribute in some fashion to episodic memory [3, 4].

Anatomical and behavioral results suggest the existence of two streams of information that converge in the hippocampus [5–7]. According to this widely accepted view, one stream conveys information about individual objects or items from the PER to the hippocampus through the lateral entorhinal area (LEA). The second stream conveys spatial and contextual information from the POR to the hippocampus through the medial entorhinal area (MEA). Consistent with the origin of the inputs converging in the PER and POR cortices, experimental lesion and electrophysiological studies show that these regions preferentially process information about objects and space, respectively [8–11].

1.1. Functional differentiation in the hippocampal formation

Among hippocampal formation structures, there is considerable evidence for functional differentiation [reviewed in 12, 13], even in the human hippocampus [14]. Although a full discussion is beyond the scope of this report, there is evidence that different structures contribute differently to the processing of spatial information. Experimental lesion studies of component structures indicate that damage to CA3, but not DG or CA1, impairs associative learning when spatial elements are part of the information to be learned [15, 16]. CA3 is also implicated in temporal processing of information when there is a spatial component [17]. Other work suggests that DG supports pattern separation of space and context and associations among sensory inputs with a spatial component [12, 18, 19]. CA1, however, supports temporal pattern separation and arbitrary associations with a temporal component [18, 20]. There is also evidence from electrophysiological studies that the behavior of CA1 and CA3 ensembles and place fields can be dissociated [21–24].

In addition to regional differences in function, there is functional specialization along the septotemporal or dorsoventral axis of the hippocampal formation [reviewed in 25]. Lesions of the dorsal hippocampus are associated with deficits in spatial processing [26]; whereas lesions of the ventral hippocampus are associated with impairments in emotional processing and conditioning [27, 28]. Rogers et al, [29] examined this issue more closely in CA1 using trace fear conditioning. Damage to either dorsal or ventral CA1 caused deficits in contextual freezing, but effects of ventral damage were more severe. In addition, effects of damage to ventral CA1 suggested a role in retention of trace fear conditioning. Analysis of *Arc* expression associated with spatial and nonspatial object recognition provided evidence that

NIH-PA Author Manuscript

NIH-PA Author Manuscript

NIH-PA Author Manuscript

dorsal CA1 is recruited after exposure to novel objects and novel object locations, whereas ventral CA1 is recruited primarily after exposure to novel locations [30]. *Arc* expression in dorsal and ventral CA3 was similar following exposure to novel objects and locations. Finally, there are dorsal vs. ventral differences in properties of theta oscillations and in spatial firing characteristics of place fields [31–33].

Although the hippocampus has been more extensively studied, there is evidence that the subiculum, in the hippocampal formation, and the presubiculum and parasubiculum, in the parahippocampal region, also contribute to learning and memory and other cognitive functions, e.g. object recognition, spatial processing, and affective function [34–37]. The subiculum also exhibits functional differentiation along the dorsoventral axis with dorsal subiculum contributing to processing spatial information and ventral subiculum contributing to affective functions [reviewed in 38].

1.2. Connections among hippocampal and parahippocampal structures

There are prior descriptions of connections among hippocampal and parahippocampal structures [reviewed in 39, 40, 41]. The entorhinal connections with hippocampal formation structures have been most thoroughly studied, especially the topography of the entorhinal projections to the DG and CA fields [42–45]. Steward and Scoville [46] first reported that the entorhinal projections to the DG and CA3 arose in layer II and that the projections to CA1 and subiculum arose in layer III. A number of studies have since addressed the entorhinal connections with CA1 and subiculum in greater detail [e.g. 44, 47–49].

There is neuroanatomical differentiation along the dorsoventral axis of the hippocampus proper [42, 50, 51]. Analysis of retrograde tract tracer injections along the dorsoventral axis of the DG, revealed that injections in the dorsal half of the DG labeled cells that occupied layer II of the most lateral part of the LEA and the most caudomedial part of the MEA [42]. This area was termed the lateral band (Figure 2B). Injections into the third dorsoventral quarter of the DG resulted in labeled layer II cells in a strip of entorhinal cortex lying adjacent to the lateral band, termed the intermediate band. Injections into ventral quarter of the DG resulted in labeled layer II cells in the medial aspect of the lateral entorhinal area and as well as the rostral and medial aspect of the medial entorhinal area, a region termed the medial band. A followup study determined that the intrinsic projections of the entorhinal cortex were related to the DG-projecting bands of origin [52]. Local connections of projection cells located in the lateral band were found to terminate in the lateral band, spanning the LEA and MEA. The same was true for the intermediate and medial bands, and this was the case whether injection sites were confined to deep or superficial layers. Thus, entorhinal cells that project to the dorsal DG are not interconnected with cells that project to the ventral DG, suggesting that information processing in different components of the entorhinal-hippocampal circuitry can proceed somewhat independently. The relative strength of the return projections to the different bands has not been addressed.

Neither the POR nor the PER projects directly to the DG or to CA3 [43, 51, 53, 54]. Prior studies have provided evidence that the PER projects to the CA1 and that both PER and POR are reciprocally connected with the subiculum [51, 54]. Whether the POR also projects directly to the CA1 and the relative strengths of these connections has not been thoroughly documented.

Given the functional and anatomical differentiation in the hippocampal formation and along the dorsoventral axis, it would be useful to directly compare connections of the PER, POR, LEA, and MEA with dorsal and ventral components of the hippocampal formation as well as with dorsal and ventral presubiculum and rostral and caudal parasubiculum. The present study examined these connections using quantitative and semiquantitative methods. We also

NIH-PA Author Manuscript

NIH-PA Author Manuscript

NIH-PA Author Manuscript

examined LEA and MEA connectivity with respect to the lateral, intermediate, and medial DG-projecting bands.

2. Materials and methods

2.1. Subjects

Forty-six male Sprague-Dawley rats, aged 2–3 months and weighing between 300–400g at the time of surgery served as subjects; anatomical data from some of these cases has been described in previous experiments [55, 56]. Subjects were initially housed in groups of 2–4 under standard 12:12 hr light:dark conditions and given *ad libitum* access to food and water. Postoperatively, all animals were housed individually so as not to jeopardize sutures in the scalp wound. Methods involving the use of live laboratory rats conformed to NIH guidelines and were approved by the appropriate institutional care and use committee.

2.2. Surgery

Surgery procedures were as previously reported [55, 56]. Briefly, animals were anaesthetized with injectable or gas anesthesia and secured in a stereotaxic apparatus (Kopf, Tujunga, CA). An incision was made in the scalp and the connective tissue was retracted. Using a dental drill, craniotomies were made in the skull dorsal to the intended injection sites. A small incision was then made in the dura to allow insertion of the micropipette without breakage. Each subject received from one to three injections of anterograde and/or retrograde tract tracers. Thirty-four rats received a single injection. Twelve rats received two retrograde tracer injections in the same hemisphere in two different regions. Two of those twelve rats also received an anterograde injection in the opposite hemisphere. Coordinates of the intended cortical targets were taken from Paxinos and Watson (1998).

The anterograde tracers, biotinylated dextran amine (BDA) or *Phaseolus vulgaris*-leuccoagglutinin (PHA-L), were delivered to either the PER (n=10), POR (n=5), LEA (n=8) or MEA (N=6). BDA was prepared as a 10% solution in 0.1 M phosphate buffered saline (PBS). PHA-L was prepared as a 2.5% solution in 0.1 M PBS. Tracers were injected through the glass micropipettes using iontophoresis with 8 min of positive DC current (4 μamps; 8 seconds on, 8 seconds off). Micropipettes had an average tip diameter of 4–5 μm.

The retrograde tracers (Dr. Illing GmbH and Co., Gross Umstadt, Germany) Diamidino Yellow (DY) or Fast Blue (FB) were injected to either the PER (n=11), POR (n=6), LEA (n=8), and MEA (n=6). Diamidino Yellow was prepared in a 2% solution in distilled water and FB was prepared in a 3% solution in distilled water. Tracers were pressure injected through a glass micropipette, with a tip diameter ranging from 60–90 μm [57].

Following the injection procedure, the wound was sutured, and the animal was visually monitored, periodically, for several hours. Once subjects were awake and had demonstrated the righting reflext, they were returned to the colony for a variable survival period depending on the tracers injected. Survival was 7–9 days for retrograde tracers and most anterograde tracers. A few animals (5) injected with BDA, only, were allowed to survive 10–14 days, labeling in these cases did not differ from other cases. Injection site size was quantified, but size of the injection site was not a reliable indicator of success of transport.

2.3. Tissue processing

Subjects were deeply anesthetized with either a 35% solution of chloral hydrate or an intraperitoneal injection of Beuthanasia (Schering-Plough, Kenilworth, NJ). Animals were transcardially perfused using a pH shift protocol; all solutions were perfused at a flow rate of 35–40 ml/minute [58]. An initial two-minute perfusion of 23°C saline was followed by 10

NIH-PA Author Manuscript

NIH-PA Author Manuscript

NIH-PA Author Manuscript

min of 4% paraformaldehyde in 0.1 M sodium acetate buffer (pH 6.5 at 4°C) and 15 min of 4% paraformaldehyde in 0.1 M sodium borate buffer (pH 9.5 at 4°C). Ice was packed around the subject's head to cool the brain throughout the perfusion procedure. The brains were removed from the skull, postfixed for 6 hours in the final fixative and cryoprotected for 24 hours in 20% glycerol in 0.02 M potassium phosphate buffered saline (KPBS, pH 7.4 at 4°C). The brains were either frozen and stored at −70°C or frozen for immediate sectioning.

Brains were cut into five series of 30 μm sections on a freezing microtome. Sectioning began at the rostral limit of the prefrontal cortex and extended through the caudal pole of the neocortex. Two of the 1:5 series were used for retrograde or anterograde tracer processing. A third series was mounted and stained for Nissl using thionin. The remaining two series were either used for other procedures or were stored at −70°C in cryoprotectant consisting of 30% ethylene glycol and 25% glycerol in sodium phosphate buffer [for details, see 58].

2.4. Reagents

2.4.1. Anterograde tracers—BDA labeled fibers were visualized using an avidin-biotin reaction. Sections were initially pre-treated in a 1% solution of triton-X 100 (TX) in KPBS for 1 hour in order to facilitate penetration of reagents. Subsequently, sections were incubated at 4°C overnight in a solution of avidin reagent (1:25 dilution) and stabilizer (1:50 dilution) from a Super ABC Kit (Biomeda Corporation) in KPBS and 0.1% solution of TX. Following three, 10 minute washes in KPBS, the sections were incubated in 0.05% diaminobenzidine (DAB; Pierce, Tacoma, WA) plus 0.04% hydrogen peroxide in KPBS for 10–30 min for the visualization of fibers.

A biotinylated secondary antibody, with an avidin-biotin incubation [59], was used to visualize PHA-L labeled fibers. Tissue was initially incubated for 2–3 hrs in 5% normal goat serum (NGS) and 0.5% TX 100 in KPBS to minimize non-specific binding. Sections were then incubated in the primary antiserum solution of rabbit anti-PHA-L (1:12,000 dilution; Dako, Carpenteria, CA) in 0.3% TX and 2% NGS in KPBS for 42–48 hrs. Following two 10 minute washes in 2% NGS in KPBS, sections were incubated in the biotinylated secondary antibody solution of goat anti-rabbit IgG (1:277 dilution; Vector Laboratories, Burlingame, CA), 0.3% TX, and 2% NGS in KPBS for 1 hr. Sections were then washed twice in 2% NGS in KPBS and incubated in a solution of avidin reagent (1:100 dilution) and stabilizer (1:200 dilutions) using a Super ABC Kit (Biomeda Corporation, Foster City, CA) in KPBS for 45 min. Following two 10 minute washes in 2% NGS in KPBS, tissue was placed into the biotinylated secondary solution for 45 min. Sections were placed in two 10 min washes in KPBS, followed by 30 min incubation in the avidin. After three 10 min washes in KPBS, sections were processed for visualization by a 5–10 min incubation in 0.05% DAB (Pierce, Tacoma, WA) plus 0.04% hydrogen peroxide in KPBS.

Following completion of all immunohistochemistry procedures, the sections were washed in KPBS, mounted on gelatin coated slides, dried in a 40°C oven, defatted, and intensified with either gold chloride [61] or with osmium tetroxide and thiocarbohydrazide [60].

2.4.2. Retrograde tracers—Sections analyzed for fluorescence were mounted onto gelatin-coated slides immediately after sectioning. The mounted tissue was dried for 2–4 hours at room temperature in a vacuum dessicator. The sections were then dehydrated in 100% ethanol (2 × 2 min), cleared in xylene (3 × 2 min), and coverslipped with DPX Mountant (Gallard-Schlessinger, Plainview, NY).

NIH-PA Author Manuscript

NIH-PA Author Manuscript

NIH-PA Author Manuscript

2.5. Data analysis

2.5.1. Anterograde analysis—Regional borders for areas within the hippocampal formation and subiculum were determined based on Swanson [62]. Each hippocampal formation structure was further subdivided into dorsal and ventral halves for anatomical analysis [42].

PHA-L- and BDA-positive fibers and terminal labeling were analyzed using darkfield optics. Fibers in the hippocampus proper, subiculum, presubiculum, and parasubiculum were rated for density of label on a subjective scale of 0–6. A score of zero indicated no fiber labeling, a score of 1 indicated negligible labeling, while scores from 2 to 6 indicated very sparse to very dense fiber labeling. Density scores were averaged across PER area 35, area 36, POR, LEA, and MEA injection sites and analyzed to identify differences in patterns of anterograde labeling in the target hippocampal formation and parahippocampal structures.

2.5.2. Retrograde analysis—Contours were drawn for a 1:10 series of sections ipsilateral to the injection site at low magnification. When FB and DY were used in the same case, double-labeled cells were easily identified as DY labels the nucleus with yellow and FB labels the cytoplasm with blue. Labeled cells were then plotted at a magnification of 100X using a Nikon Optiphot-2 or Nikon E600 coupled to a semi-automated data collection system (Neurolucida, Microbrightfield, Inc., Burlington, VT). For each section, the area of each contour and the total number of cells within the contour were quantified by Neurolucida and exported to Excel (Microsoft, Inc). The total number of cells in each region was estimated by multiplying by 10. Values for each set of injection sites were normalized to the mean across all cases of the total number of labeled cells in a set of structures including all cortical, subcortical, and hippocampal structures [63, 64]. This procedure was applied to ensure that our results would not be biased by differences in transport across cases. Briefly, the total number of labeled cells was calculated for each case, the mean for all cases was obtained, and a correction factor was calculated by dividing the total for each case by the mean total for all cases. This correction factor was applied to the number of cells labeled in each region. The volume of each afferent region was estimated by summing the areas of the contours and multiplying by 10.

The density of labeled cells was calculated as the total normalized number of cells in each region divided by the volume of the region. Estimates may be biased by increased probability of double counting along the z axis as well as by loss of caps due to the difficulty in identifying partial cell bodies at the margin of a coronal section. These biases, however, are not likely to significantly impact the interpretation of results; the biases are in opposite directions and estimates of cell number and density in all regions were subject to the same bias.

2.6. Nomenclature

Borders for the PER and POR were taken from Burwell [58]. For the entorhinal cortex, we relied on classical descriptions of the region that subdivide the area into the LEA and the MEA [65–67]. Together the PER, POR, and entorhinal cortices occupy the lateral, ventrocaudal, and caudal surfaces of the rat brain. The PER is a rostrocaudally oriented strip of cortex associated with the rhinal sulcus (Figure 2). The PER comprises two subregions, areas 35 and 36, with area 36 lying dorsal to area 35. The dorsal border of area 36 is with ventral temporal cortex. The POR is located caudal to the PER and is dorsal to the caudal extension of the rhinal sulcus. The rhinal sulcus at this rostrocaudal level is occupied by the entorhinal cortex [52]. The POR is bordered dorsally by visual association cortex and ventrally by the MEA and parasubiculum. The LEA is rostral and lateral to the MEA. Its dorsolateral border is close to the rhinal sulcus. Ventrally, the LEA is bordered by piriform

NIH-PA Author Manuscript

NIH-PA Author Manuscript

NIH-PA Author Manuscript

cortex at rostral levels, periamygaloid cortex at mid-rostrocaudal levels, and the MEA at caudal levels. The MEA is bordered dorsally by the POR and parasubiculum, laterally by ventral LEA, and medially by parasubiculum.

Preliminary analyses of data presented here were included in prior commentaries in summarized form such that data were aggregated across cases and summarized for composite regions [63, 64]. Here we present the results of detailed analyses of the subdivisions of the hippocampal formation and the parahippocampal structures.

The term hippocampal system includes the hippocampal formation and the parahippocampal region. The hippocampal formation includes the DG, the CA fields of the hippocampus proper (CA3, CA2, and CA1), and the subiculum (Figure 1). These regions are strongly interconnected, as described by the classic illustration of the trisynaptic loop. Prior anatomical work has distinguished the components of the hippocampal formation from the parahippocampal region, based on cortical structure [2]. The DG, CA fields, and subiculum have a three layer structure, whereas structures in the parahippocampal region contain more than three layers [68]. Individual components of the hippocampal formation were further subdivided into dorsal and ventral subfields for anatomical analysis according to the septotemporal topography of the perforant pathway projections described by Dolorfo and Amaral [42].

The parahippocampal region includes the PER, POR, LEA, MEA, the presubiculum, and the parasubiculum [2]. Additionally, the presubiculum included the most dorsal extent of the region, sometimes termed the postsubiculum [69, 70]. For analysis, the presubiculum was subdivided into dorsal and ventral subfields, and the parasubiculum was subdivided into rostral and caudal subfields.

3. Results

3.1. Description of injection sites

Anterograde and retrograde tracers were injected into the PER areas 35 and 36, POR, LEA, and MEA. Locations of all injection sites are represented on unfolded maps of the target regions (Figure 2C and 2D). Representative examples of injection sites are shown in Figure 3. Information about size, location, and laminar location of the anterograde and retrograde injection sites are shown in Tables 1 and Table 2, respectively. The area of the anterograde injection site was defined as the region containing labeled cell bodies in the coronal section in which the area was largest. The size of a retrograde tracer injection site was defined as the region that included the dye core and the surrounding halo in the coronal section in which the area was largest.

For anterograde injections (Table 1), nearly all sites involved both deep and superficial layers. One POR site and three LEA sites appeared to include only superficial layers. Because the primary projections to hippocampal structures arise in superficial layers, these cases were retained for quantitative analysis. Two POR cases involved only deep layers, and yielded no labeling in any hippocampal or parahippocampal structure. Data from these cases is not included in tables. There were also three entorhinal sites that had little or no involvement with layer II. These cases were removed from quantitative analyses and so data are also not included in tables.

For retrograde injections (Table 2), most sites involved deep layers or superficial and deep layers. For the PER, there was one injection site in area 36 that was restricted to superficial layers, 99DY. This site yielded no labeled cells in any hippocampal or parahippocampal structure, and thus was removed from quantitative analyses reported in Tables 3 and Table

NIH-PA Author Manuscript

NIH-PA Author Manuscript

NIH-PA Author Manuscript

4. For the remaining areas, area 35, POR, LEA, and MEA, most retrograde injections involved both superficial and deep layers, but two sites in each region appeared to be restricted to layer V. These were retained for quantitative analyses as the return projections primarily target deep layers.

3.2. Pathways

Fibers from injection sites in the PER areas 35 and 36, POR, LEA and MEA, were observed to enter the external capsule or angular bundle. After traveling a distance, fibers were observed to exit via the alvear and dorsal hippocampal commissure to innervate hippocampal structures. Entorhinal fibers were also observed to cross the subiculum in the perforant path. Although contralateral connections were not evaluated in the present paper, we do report that fibers of passage crossed to the hemisphere opposite the injection site through the corpus callosum and through the temporal limb of the anterior commissure.

3.3 Perirhinal and postrhinal cortices

3.3.1. PER and POR projections to hippocampal and parahippocampal structures—Based on assessments of fiber labeling following anterograde tracer injections, areas 35 and 36 provide only light projections to hippocampal structures (Table 3). The two cases involving only deep layers (54P and 90P) did not result in any labeling in hippocampal or parahippocampal areas and so are not included in Table 3. This confirms, however, that the projections arise in superficial layers. Both area 35 and area 36 provide light input to ventral subiculum. Area 36 also provides a light input to ventral CA1, dorsal presubiculum, and rostral and caudal parasubiculum. A few labeled fibers were observed in other regions, including CA2 and ventral CA3 arising from area 36 injections, but this level of labeling is considered negligible.

Fiber labeling in hippocampal structures arising from tracer injections in the POR was more substantial than that arising from PER areas 35 and 36, but still light. Area 36 projects lightly to dorsal CA1, as well as dorsal and ventral subiculum (Table 3). POR projections to hippocampal structures were lighter than those arising from either of the two entorhinal subdivisions. The strongest projections from POR were to the dorsal presubiculum (Figure 4) and the caudal parasubiculum. In contrast, labeling in ventral presubiculum and rostral parasubiculum was sparse.

3.3.2. Hippocampal and parahippocampal projections to PER and POR—Based on densities of labeled cells arising from PER retrograde tracer injections, overall, hippocampal and parahippocampal structures project more heavily to area 35 than to area 36 (Figure 5A and 5B). The one case that did not involve deep layers (90DY) resulted in no labeled cells in any structure. Thus, input targets deep layers. Input was also stronger, overall, from ventral as compared to dorsal regions (Table 4). There is essentially no projection to areas 35 and 36 arising in the DG. Likewise, density of labeled cells in dorsal and ventral CA3 and CA2 was either very light or observed only in a single case. Following area 35 injections, ventral CA1 and ventral subiculum were most densely labeled. Dorsal subiculum and rostral parasubiculum were also densely labeled. Following area 36 injections, again, ventral CA1 was most densely labeled, though not as densely as for area 35 injections (see Figure 5A and 5B for comparison).

In general, the dorsal subiculum provides the strongest hippocampal input to the POR (Table 4). Compared with area 35, the POR receives greater input from dorsal CA1 and about the same from dorsal subiculum. Input from ventral CA1 and subiculum are weaker than that to either area 35 or area 36. Based on patterns of retrogradely-labeled cells, the caudal parasubiculum targets POR very heavily, much more heavily than any of the other regions

NIH-PA Author Manuscript

NIH-PA Author Manuscript

NIH-PA Author Manuscript

examined (Figure 5C). Dorsal presubiculum also provides substantial input to POR, stronger than it provides to either area 35 or area 36.

We also examined the percentage of input quantified as the percent of total number of labeled cells in the afferent structures (Table 5). For PER area 35, the greatest input was from ventral CA1, which provided nearly 40% of total input from the afferent structures. The next strongest inputs were from dorsal CA1, and dorsal and ventral subiculum. The pattern was similar for area 36 except that the percentage of input from ventral CA1 was even greater, accounting for about 54% of the total. The next strongest inputs were from dorsal CA1, ventral subiculum, and caudal parasubiculum. So, even though the hippocampal/parahippocampal input to area 36 was relatively small, the input was dominated by ventral CA1.

For the POR, roughly one-third of the total input was from dorsal presubiculum and one-third was from caudal parasubiculum (Table 5). About one-sixth of the total input was from dorsal CA1. Interestingly, there was a rostrocaudal topography of the POR connections with CA1 and dorsal presubiulum such that caudal POR injections resulted in heavier labeling in these areas. Ventral hippocampal structures provided much smaller proportion of the input to POR as compared to PER areas 35 and 36.

3.4. Entorhinal cortex

3.4.1. LEA and MEA projections to hippocampal and parahippocampal structures—LEA anterograde injections produced similar levels of labeled fibers in dorsal and ventral hippocampal and parahippocampal structures (Figure 6A and Table 3). A few cases located in the lateral band (21P, 127B, and 28P) did not include layer II, and did not result in labeling in the DG. Data from these cases are excluded from the anterograde data tables. In general, fiber labeling arising from injections in the MEA was slightly heavier to dorsal hippocampal regions as compared to that arising from injections in the LEA. In addition, MEA projections to dorsal hippocampal structures were heavier than those to the ventral hippocampal structures (Figure 6B). It should be noted, however, that differences in projections based on the DG-projection bands account for greater differences than do the LEA and MEA subdivisions, overall (see section 3.4.3.). For the parahippocampal structures, LEA injections produced the most labeling in the dorsal presubiculum and MEA injections produced the most labeling in the caudal parasubiculum.

3.4.2. Hippocampal and parahippocampal projections to LEA and MEA—The pattern of input to the LEA and MEA arising from the hippocampal and parahippocampal structures were different based on relative densities of retrogradely-labeled cells (Table 4). Ventral hippocampal structures appear to target the LEA much more strongly than dorsal hippocampal structures do. Surprisingly, the MEA projections to dorsal structures were not substantially stronger than to ventral structures. However, comparison of the two target regions reveals that dorsal structures provide stronger input to the MEA than to the LEA. Based on densities of labeled cells, dorsal CA2, dorsal CA1, and dorsal subiculum target the MEA more strongly than they target the LEA (Table 4). The complementary pattern is true for ventral structures; ventral CA3, CA2, CA1 and subiculum target the LEA more strongly than they target the MEA. In addition, ventral subiculum provides heavier input to LEA than does dorsal subiculum (Figure 7A, Table 4). Numbers of labeled cells in DG were so low as to be considered negligible. As was true for the anterograde experiments, however, examination of connections according to DG-projection bands must also be considered (see section 3.4.3.).

Overall, presubiculum and parasubiculum target the MEA more strongly than they target the LEA. Within LEA and MEA, however, we also observed an interesting complementary

NIH-PA Author Manuscript

NIH-PA Author Manuscript

NIH-PA Author Manuscript

pattern of labeling in the parahippocampal structures. For the MEA, dorsal presubiculum and caudal parasubiculum provide much stronger input than ventral presubiculum and rostral parasubiculum (Figure 7B). The opposite pattern was evident for the LEA; ventral presubiculum and rostral parasubiculum provided stronger input to the LEA than dorsal presubiculum and caudal parasubiculum.

Based on percentages of total numbers of labeled cells, by far the strongest input to the LEA arises in ventral CA1 accounting for 42% of labeled cells (Table 5). The next strongest input arises in ventral subiculum with 18% followed by dorsal CA1 with 13% of the total number of labeled cells and dorsal subiculum with 6% of labeled cells. For the MEA, the strongest inputs arise in dorsal CA1 (23%), followed by dorsal presubiculum, and caudal parasubiculum, each accounting for about 20% of total input (Table 5). Next strongest inputs were from ventral CA1 and subiculum, each accounting for 11% and 9% total input, respectively.

3.4.3. Connections of the dentate gyrus-projection bands

3.4.3.1. Projections of entorhinal bands to hippocampal and parahippocampal structures: Densities of fiber labeling arising from injection sites in the LEA and MEA lateral, intermediate, and medial DG-projecting bands are shown in Table 6. For the MEA, we were not able to place an injection in the intermediate band. Case 653B appeared to involve both the lateral and intermediate bands, but like other lateral band cases, fiber labeling was stronger in dorsal than ventral hippocampal structures. As expected based on prior literature [42], heavy projections to the dorsal hippocampal structures tend to arise from the lateral band of the LEA and the MEA, whereas heavier projections to the ventral hippocampal structures tend to arise in the intermediate and medial bands.

We also compared densities of fiber labeling in the pre- and parasubiculum arising from LEA and MEA (Table 6). In general for the LEA, the lateral and intermediate bands provide heavier input to the dorsal and ventral presubiculum than does the medial band. In contrast for the MEA, the lateral band provides greater input to dorsal presubiculum than does the medial band, but medial band provides more input to ventral presubiculum than dorsal presubciulum. For both the LEA and the MEA, the lateral band appears to target the rostral parasubiculum more strongly and the medial band targets the caudal parasubiculum more strongly. Overall, the MEA projection to the parasubiculum is stronger than that of the LEA.

3.4.3.2. Hippocampal and parahippocampal projections to entorhinal bands: An examination of the average densities of labeled cells arising from LEA and MEA injections located in different DG-projecting bands is particularly informative (Table 7). For the LEA sites in all bands, density of labeling in each ventral hippocampal structure was greater than its dorsal partner. The difference is by far the greatest for LEA sites in the medial DG-projecting band. MEA exhibits a different pattern; for the MEA sites in the lateral band, density of retrogradely-labeled cells in each dorsal hippocampal structure is greater than its associate ventral subdivision. For sites in the intermediate and medial bands, however, labeling is heavier in ventral structures. This is especially striking for the MEA medial band. Thus, dorsal hippocampus appears to be most heavily innervated by the MEA lateral band, whereas the ventral hippocampus is most heavily innervated by the medial bands of the LEA and the MEA, but also receives strong input from the LEA lateral and intermediate bands.

Another interesting comparison of LEA and MEA is in the densities of labeled cells in parahippocampal structures. Following injections in the lateral band of the LEA, the parahippocampal structures are all moderately densely labeled (Table 7, first data column). From sites in the LEA intermediate band parasubiculum is more heavily labeled. From sites in the LEA medial band, labeling is much heavier in the ventral presubiculum and the rostral

NIH-PA Author Manuscript

NIH-PA Author Manuscript

NIH-PA Author Manuscript

parasubiculum. In contrast, following injections in the lateral band of the MEA, the dorsal presubiculum and caudal parasubiculum are massively labeled — much more heavily than the ventral presubiculum and the rostral parasubiculum (Table 7). The opposite pattern is true for the input from the medial band. Similar to the LEA medial band, the MEA medial band receives much stronger input from the ventral presubiculum and rostral parasubiculum as compared with the dorsal presubiculum and caudal parasubiculum.

We also assessed input to the DG-projecting bands in terms of percentages of total labeled cells (Table 8). Based on this measure, all three LEA bands receive a greater proportion of input from ventral CA1 and subiculum as compared with dorsal CA1 and subiculum. In contrast, the lateral band of the MEA receives greater input from dorsal CA1 and subiculum, whereas the medial band receives more input from the ventral CA1 and subiculum.

Surprisingly, we found evidence for a direct projection to both the LEA and MEA arising from ventral CA3. All three injection sites located in the medial band resulted in retrogradely labeled cells in ventral CA3. These cases also resulted in some labeling in dorsal CA3. The same three cases were responsible for the bulk of labeling observed in CA2, although injection sites in other bands also produced some CA2 labeling.

4. Discussion

4.1 Summary of findings

We previously quantified the connections among the PER areas 35 and 36, POR, LEA and MEA [71]. In other studies, we have described the cortical efferents and afferents of these regions [55, 56]. Using the same quantitative and semiquantitative methods, we have now extended our studies to include the reciprocal connections of the PER areas 35 and 36, POR, LEA, and MEA with the hippocampal formation, the presubiculum, and the parasubiculum. Ours is the first study that permits direct comparisons across PER, POR, LEA and MEA of strength and patterns of reciprocal connections with hippocampal formation and subicular regions. Although we did not address the proximodistal topography of hippocampus and subiculum connections, we did examine connections with regard to the dorsoventral or septotemporal axis of the hippocampal formation. We assessed anterograde and retrograde labeling in the dorsal half of the hippocampal formation structures, which receives input from the lateral entorhinal band, and in the ventral half of the hippocampal formation structures, which receives input from the intermediate and medial entorhinal bands.

We found that the LEA and MEA projections to the hippocampal formation are much stronger than the PER and POR projections. The LEA and MEA project strongly to all components of the hippocampal formation, whereas the PER and POR project weakly and only to CA1 and the subiculum. The PER targets ventral CA1 and subiculum, whereas the POR preferentially targets the dorsal CA1 and subiculum. Similarly, the PER receives more input from ventral hippocampal formation structures and the POR receives more input from dorsal hippocampal structures. The MEA medial band and the LEA are more strongly interconnected with ventral hippocampal structures, whereas the MEA lateral band is more interconnected with dorsal hippocampal structures. Also, the dorsal presubiculum and caudal parasubiculum preferentially target the POR and the lateral band of the MEA. In contrast, the ventral presubiculum and rostral parasubiculum preferentially target the LEA and MEA medial bands. Finally, we found evidence for a direct projection from ventral CA3 to the medial band of the entorhinal cortex.

4.2 Parallel pathways through the hippocampal formation

The PER projects more strongly to the LEA, and the POR projects more strongly to the MEA [72–74], but the PER and POR also provide parallel direct inputs to the hippocampus

NIH-PA Author Manuscript

NIH-PA Author Manuscript

NIH-PA Author Manuscript

[50, 75, 76]. Here we used anterograde tracer methods to directly compare the relative strengths of those inputs. We show that the LEA and MEA projections to the hippocampal formation are much stronger than the PER and POR connections (Table 3). Moreover, the entorhinal cortex projects strongly to all components of the hippocampal formation, whereas the PER and POR project weakly and only to CA1 and the subiculum.

Although the PER and POR projections are relatively weak and restricted, available evidence suggests these projections are functionally important. Witter et al [74] suggested that the parallel sets of pathways, which begin with the PER and POR cortices, provide the hippocampal formation with functionally different inputs that are processed at three different levels of hippocampal system circuitry, resulting in three representations of the same information that differ in the amount of processing. The direct pathways, i.e. from the PER or POR, would provide relatively unprocessed information. The multi-synaptic pathways from the PER or POR, arriving at the hippocampus via the entorhinal cortex, or arriving at the entorhinal cortex after processing through the trisynaptic loop, would provide the most highly processed representation.

Our results suggest that the direct pathways arriving from the PER and POR may be biased for processing different types of information (see section 4.3).

4.3 Anatomical and functional segregation along the dorsoventral axis

The PER and POR projections to the hippocampal formation both terminate in dorsal and ventral components; however, the PER projection is stronger to ventral CA1 and subiculum, whereas the POR projection is stronger to dorsal CA1 and subiculum. Based on densities of retrogradely labeled cells, the relative strengths of the return projections to the PER and POR appear much more robust than the forward projections, though not as strong as projections to the LEA and MEA (Table 4). PER receives the strongest hippocampal input from ventral CA1 and subiculum, whereas the POR receives the strongest hippocampal input from dorsal CA1 and subiculum.

Based on percentages of retrogradely labeled cells, the patterns of input to PER areas 35, 36, and LEA were similar and the patterns of input to the POR and MEA were similar (Table 5). Areas 35, 36, and LEA receive more input from ventral hippocampal structures, whereas the POR and MEA receive more input from dorsal structures. In addition, the POR and MEA both receive more input from the dorsal presubiculum and the caudal parasubiculum and less from the ventral presubiculum and rostral parasubiculum. We subjected the percentages of input shown in Table 5 to a Pearson correlation analysis and found that Areas 35, 36, and LEA were highly intercorrelated (r's ranged from 0.92 to 0.97, $p < 0.0001$). Percentages of input to the POR and MEA were also highly correlated ($r = 0.88$, $p < 0.0001$). No other correlations were significant. The results of this analysis are consistent with descriptions of the spatial and nonspatial processing streams; however, the data shown in Table 5 obscure the effects of intrinsic connections that span LEA and MEA.

Evaluation of the projections arising from the LEA and MEA intrinsic connectivity bands were largely consistent with earlier findings [42], in that the lateral bands projected more strongly to dorsal than ventral structures and the medial bands more strongly to ventral than dorsal structures (Table 6). We assessed the similarities of inputs to the different intrinsic connectivity bands for the LEA and MEA using the same correlation method described above. That is, we subjected the percentages of input shown in Table 8 to a Pearson correlation analysis. We found that the LEA lateral, intermediate, and medial bands and the MEA medial band were all highly intercorrelated (r's ranged from 0.75 to 0.92, p's < 0.0002). No other correlations were significant. This suggests that ventral hippocampal

NIH-PA Author Manuscript

NIH-PA Author Manuscript

NIH-PA Author Manuscript

structures exert control over not just the LEA and MEA medial bands, but also the LEA lateral and intermediate bands.

Studies of the effects of damage to the ventral hippocampus, in particular ventral CA1, suggest a role in emotional learning. Ventral hippocampal lesions cause behavioral deficits in an auditory fear conditioning paradigm [28, 29]. Other evidence suggests the ventral subiculum contributes to the regulation of the hypothalamic pituitary axis and stress response [37]. Thus based on its hippocampal connections, the LEA as a whole may have a greater role in emotional processing than previously understood. This is likely also true for the PER. In addition to its connections with ventral hippocampal structures, subcortical connections of the PER are consistent with a role emotional memory and reward processing; PER is strongly and reciprocally connected with the amygdala nuclei [77, 78]. Here we show that the PER receives afferent input from, and provides efferent projections back to, the ventral subiculum. Taken together, the evidence suggests that the connections of the PER, the LEA, and the medial band of the MEA are consistent with a role for these regions in emotional learning mechanisms.

4.4 Evidence for direct projections from CA3 to the entorhinal cortex

Consistent with a few earlier studies, we found evidence for a direct projection from the CA3 to the medial band of the entorhinal cortex. Following retrograde tracer injections involving deep layers of the medial band in either the LEA or the MEA, a substantial number of cells were labeled in the ventral CA3 (Table 7). Though substantially fewer, there were also cells labeled in dorsal CA3 arising from the same cases. This pattern of labeling was evident in all three injection sites that were located in the medial DG-projecting band, i.e. the part of the entorhinal cortex that projects to the fourth quarter of the DG and CA3. Only cases with injection sites located in the medial band resulted in labeled cells in CA3. These cases also produced the predominance of the labeling we observed in ventral CA2, although sites located in other bands did result in a lower density of retrogradely labeled cells in ventral and dorsal CA2.

There are earlier reports of a direct projection from CA3 to the entorhinal cortex [79, 80]. Using early fiber degeneration techniques, Hjorth-Simonsen [81] found evidence for a projection from the ventral or temporal third of CA3 to layer IV of the MEA. Using the retrograde tracer, horseradish peroxidase (HRP), Beckstead [82] reported HRP-positive cells in the ventral two-thirds of CA3 following injections in the LEA, but no labeled cells following injections in the MEA. Using autoradiography, an anterograde tract-tracing technique, Swanson and colleagues [83, 84] reported that ventral or septal CA3 projected to both the LEA and the MEA. We have now replicated that finding using retrograde tract tracing methods.

Although the CA3-entorhinal projection requires more study, there are implications for the information processing in the ventral hippocampus and medial entorhinal band. For example, it may be that a direct projection from the CA3 to the medial band of the LEA supports the rapid association of emotional information with place and time.

4.5 PER, POR, LEA, and MEA connections with presubiculum and parasubiculum

Not much is known about the connections of the PER and POR with presubiculum and parasubiculum, although those of the LEA and MEA are well studied [79, 80]. We found that the POR was strongly and reciprocally connected with the dorsal presubiculum and caudal parasubiculum. PER area 36, but not area 35, provided light inputs to presubiculum or parasubiculum. The return projection to PER was heaviest from rostral parasubiculum to area 35.

NIH-PA Author Manuscript

NIH-PA Author Manuscript

NIH-PA Author Manuscript

We found that both the LEA and the MEA project to the presubiculum and the parasubiculum [see also 85, 86]. This is not consistent with some prior reports that the MEA, but not the LEA, projects to these structures [87–89]. As reported previously [90–92], we also found that the presubiculum and parasubiculum project back to the LEA and MEA.

These findings have important functional implications given that grid cells were recorded in the presubiculum [93], and that place cells and grid cells have been recorded in the parasubiculum [93, 94]. The dorsal presubiculum is known to process information about head direction and landmarks [reviewed in 95]. Inactivations of presubiculum disrupted performance on object location tasks and disrupted place fields recorded from dorsal hippocampus [96]. Lesions of the presubiculum and parasubiculum impaired performance on spatial working memory and object location [34], but this could be attributed to presubicular damage as the efferents and afferents of the pre and parasubiculum are distinctly different [97]. Object location information has been observed in the POR [98]. Most likely object information arises directly from the PER, but it is also possible that object-location information comes from the presubiculum and/or the parasubiculum.

Here we show that the MEA lateral band receives a massive input from the dorsal presubiculum and the caudal parasubiculum and a much smaller input from the ventral presubiculum and rostral parasubiculum. A similar pattern is evident for the POR. Though not as extreme, the opposite pattern is evident for the MEA and LEA medial bands. This suggests that the dorsal presubiculum and the caudal parasubiculum may be important for spatial functions of the POR and the lateral band of the MEA. In contrast, the ventral presubiculum and rostral parasubiculum connections with the LEA and MEA medial bands may be more important for non-spatial functions.

4.6 Implications for the spatial and nonspatial processing streams

Although there has been substantial emphasis on the POR-MEA spatial processing stream and the PER-LEA non-spatial stream, the associated pathways are not strictly segregated. The PER does project primarily to the LEA, but caudal PER also provides a weak projection to the MEA; in addition, the POR projects to caudal LEA as well as to MEA [71]. The LEA and MEA connections are problematic as well because bands of intrinsic connectivity in the entorhinal cortex span the LEA and the MEA [52]. We show here that POR and PER projections are biased toward dorsal and ventral halves of the hippocampus, respectively (Table 3). In addition, the POR and PER projections to the LEA and MEA are strongest to the lateral band, but both structures also provide weaker input to the intermediate and medial bands [71]. On the output side, we confirmed in the present study that the LEA and MEA lateral bands preferentially target dorsal hippocampal structures, whereas the LEA and MEA medial bands preferentially target ventral hippocampal structures [see also 42].

Taken together these findings suggest that the accepted view of the spatial and nonspatial processing streams is oversimplified. The patterns of connections of the entorhinal bands and the connectivity along the dorsoventral axis of the hippocampus both have important implications for functional differentiation in the hippocampal system.

5. Conclusions

Neuroanatomic and functional connectivity studies have identified segregated spatial and nonspatial processing streams feeding into the hippocampus in rodents, monkeys, and humans [56, 99–101]. The current view is that the spatial and nonspatial processing streams target the POR-MEA and PER-LEA, respectively. Our findings suggest that view may be oversimplified and that functional differentiation along the dorsoventral axis should be taken into account. For example, the connections of the medial band of the MEA suggest its

NIH-PA Author Manuscript

NIH-PA Author Manuscript

NIH-PA Author Manuscript

functions may be more similar to the PER and LEA than to the POR and MEA lateral band. We also provide evidence that dorsal presubiculum and caudal parasubiculum are associated with the POR- lateral MEA circuitry. In contrast, the ventral presubiculum and rostral parasubiculum are more associated with the PER-LEA-medial MEA circuitry.

Our findings provide greater insight into medial temporal lobe function and suggest new testable hypotheses about medial temporal lobe circuitry. Future work should compare and contrast the subcortical connections of these areas in order to yield a complete picture of the functional neuroanatomy of these regions.

Acknowledgments

This research was supported, in part, by an NSF grant to RDB (IBN9875792) and an NRSA to KLA (MH072144). We thank Kristin Kerr-Scaplen for her careful reading of our manuscript.

References

1. Scoville WB, Milner B. Loss of recent memory after bilateral hippocampal lesions. J Neurol Neurosurg Psychiatry. 1957; 20:11–21. [PubMed: 13406589]
2. Scharfman HE, Witter MP. Preface for the parahippocampal region: Implications for neurological and psychiatric diseases. Ann N Y Acad Sci. 2000; 911:ix–xiii. [PubMed: 10911863]
3. Eichenbaum H, Yonelinas AP, Ranganath C. The medial temporal lobe and recognition memory. Annual review of neuroscience. 2007; 30:123–152.
4. Squire LR, Stark CE, Clark RE. The medial temporal lobe. Annual review of neuroscience. 2004; 27:279–306.
5. Burwell RD. The parahippocampal region: corticocortical connectivity. Ann N Y Acad Sci. 2000; 911:25–42. [PubMed: 10911865]
6. Eichenbaum H, Sauvage M, Fortin N, Komorowski R, Lipton P. Towards a functional organization of episodic memory in the medial temporal lobe. Neuroscience and biobehavioral reviews. 2012; 36:1597–1608. [PubMed: 21810443]
7. Knierim JJ, Lee I, Hargreaves EL. Hippocampal place cells: parallel input streams, subregional processing, and implications for episodic memory. Hippocampus. 2006; 16:755–764. [PubMed: 16883558]
8. Eacott MJ, Norman G. Integrated memory for object, place, and context in rats: a possible model of episodic-like memory? J Neurosci. 2004; 24:1948–1953. [PubMed: 14985436]
9. Gaffan EA, Eacott MJ, Simpson EL. Perirhinal cortex ablation in rats selectively impairs object identification in a simultaneous visual comparison task. Behavioral Neuroscience. 2000; 114:18–31. [PubMed: 10718259]
10. Norman G, Eacott MJ. Dissociable effects of lesions to the perirhinal cortex and the postrhinal cortex on memory for context and objects in rats. Behav Neurosci. 2005; 119:557–566. [PubMed: 15839802]
11. Burwell RD, Hafeman DM. Positional firing properties of postrhinal cortex neurons. Neuroscience. 2003; 119:577–588. [PubMed: 12770570]
12. Kesner RP. An analysis of the dentate gyrus function. Behavioural brain research. 2013
13. Hunsaker MR, Kesner RP. The operation of pattern separation and pattern completion processes associated with different attributes or domains of memory. Neuroscience and biobehavioral reviews. 2013; 37:36–58. [PubMed: 23043857]
14. Eldridge LL, Engel SA, Zeineh MM, Bookheimer SY, Knowlton BJ. A dissociation of encoding and retrieval processes in the human hippocampus. The Journal of neuroscience : the official journal of the Society for Neuroscience. 2005; 25:3280–3286. [PubMed: 15800182]
15. Gilbert P, Kesner RP. Localization of function within the dorsal hippocampus: the role of the CA3 subregion in paired-associate learning. Behav Neurosci. 2003; 117:1385–1394. [PubMed: 14674856]

NIH-PA Author Manuscript

NIH-PA Author Manuscript

NIH-PA Author Manuscript

16. Hunsaker M, Thorup JA, Welch T, Kesner RP. The role of CA3 and CA1 in the acquisition of an object-trace-place paired-associate task. Behav Neurosci. 2006; 120:1252–1256. [PubMed: 17201469]

17. Hunsaker MR, Kesner RP. Evaluating the differential roles of the dorsal dentate gyrus, dorsal CA3, and dorsal CA1 during a temporal ordering for spatial locations task. Hippocampus. 2008; 18:955–964. [PubMed: 18493930]

18. Gilbert PE, Kesner RP, Lee I. Dissociating hippocampal subregions: double dissociation between dentate gyrus and CA1. Hippocampus. 2001; 11:626–636. [PubMed: 11811656]

19. Schmidt B, Marrone DF, Markus EJ. Disambiguating the similar: the dentate gyrus and pattern separation. Behavioural brain research. 2012; 226:56–65. [PubMed: 21907247]

20. Kesner R, Hunsaker MR, Gilbert PE. The role of CA1 in the acquisition of an object-trace-odor paired associate task. Behav Neurosci. 2005; 119:781–786. [PubMed: 15998199]

21. Lee I, Knierim JJ. The relationship between the field-shifting phenomenon and representational coherence of place cells in CA1 and CA3 in a cue-altered environment. Learn Mem. 2007; 14:807–815. [PubMed: 18007023]

22. Lee I, Rao G, Knierim JJ. A double dissociation between hippocampal subfields: differential time course of CA3 and CA1 place cells for processing changed environments. Neuron. 2004; 42:803–815. [PubMed: 15182719]

23. Lee I, Yoganarasimha D, Rao G, Knierim JJ. Comparison of population coherence of place cells in hippocampal subfields CA1 and CA3. Nature. 2004; 430:456–459. [PubMed: 15229614]

24. Roth ED, Yu X, Rao G, Knierim JJ. Functional differences in the backward shifts of CA1 and CA3 place fields in novel and familiar environments. PLoS One. 2012; 7:e36035. [PubMed: 22558316]

25. Fanselow MS, Dong HW. Are the dorsal and ventral hippocampus functionally distinct structures? Neuron. 2010; 65:7–19. [PubMed: 20152109]

26. Moser M, EI M, E F, P A, RG M. Spatial learning with a minislab in the dorsal hippocampus. Proc Natl Acad Sci U S A. 1995; 92:9697–9701. [PubMed: 7568200]

27. Burman M, Starr MJ, Gewirtz JC. Dissociable effects of hippocampus lesions on expression of fear and trace fear conditioning memories in rats. Hippocampus. 2006; 16:103–113. [PubMed: 16261555]

28. Yoon T, Otto T. Differential contributions of dorsal vs. ventral hippocampus to auditory trace fear conditioning. Neurobiol Learn Mem. 2007

29. Rogers J, Hunsaker MR, Kesner RP. Effects of ventral and dorsal CA1 subregional lesions on trace fear conditioning. Neurobiol Learn Mem. 2006; 86:72–81. [PubMed: 16504548]

30. Sauvage MM, Nakamura NH, Beer Z. Mapping memory function in the medial temporal lobe with the immediate-early gene Arc. Behavioural brain research. 2013

31. Jung M, Wiener SI, McNaughton BL. Comparison of spatial firing characteristics of units in dorsal and ventral hippocampus of the rat. J Neurosci. 1994; 14:7347–7356. [PubMed: 7996180]

32. Kjelstrup KB, Solstad T, Brun VH, Hafting T, Leutgeb S, Witter MP, et al. Finite scale of spatial representation in the hippocampus. Science. 2008; 321:140–143. [PubMed: 18599792]

33. Royer S, Sirota A, Patel J, Buzsaki G. Distinct representations and theta dynamics in dorsal and ventral hippocampus. The Journal of neuroscience : the official journal of the Society for Neuroscience. 2010; 30:1777–1787. [PubMed: 20130187]

34. Liu P, Jarrard L, Bilkey D. Excitotoxic lesions of the pre- and parasubiculum disrupt object recognition and spatial memory processes. Behav Neurosci. 2001; 115:112–124. [PubMed: 11256435]

35. Taube J, Kesslak JP, Cotman CW. Lesions of the rat postsubiculum impair performance on spatial tasks. Behav Neural Biol. 1992; 57:131–143. [PubMed: 1586352]

36. Broussard J, Sarter M, Givens B. Neuronal correlates of signal detection in the posterior parietal cortex of rats performing a sustained attention task. Neuroscience. 2006; 143:407–417. [PubMed: 17045755]

37. O'Mara S. Controlling hippocampal output: the central role of subiculum in hippocampal information processing. Behav Brain Res. 2006; 174:304–312. [PubMed: 17034873]

NIH-PA Author Manuscript

NIH-PA Author Manuscript

NIH-PA Author Manuscript

38. O'Mara SM, Sanchez-Vives MV, Brotons-Mas JR, O'Hare E. Roles for the subiculum in spatial information processing, memory, motivation and the temporal control of behaviour. Prog Neuropsychopharmacol Biol Psychiatry. 2009; 33:782–790. [PubMed: 19393282]
39. Witter MP. Organization of the entorhinal-hippocampal system: a review of current anatomical data. Hippocampus. 1993; 3 Spec No:33–44.
40. Witter, M.; Amaral, D. The Rat Nervous System. 3 ed.. San Diego: Academic Press, Inc; 2004.
41. Amaral DG, Scharfman HE, Lavenex P. The dentate gyrus: fundamental neuroanatomical organization (dentate gyrus for dummies). Prog Brain Res. 2007; 163:3–22. [PubMed: 17765709]
42. Dolorfo CL, Amaral DG. Entorhinal cortex of the rat: topographic organization of the cells of origin of the perforant path projection to the dentate gyrus. Journal of Comparative Neurology. 1998; 398:25–48. [PubMed: 9703026]
43. Canning KJ, Leung LS. Lateral entorhinal, perirhinal, and amygdala-entorhinal transition projections to hippocampal CA1 and dentate gyrus in the rat: a current source density study. Hippocampus. 1997; 7:643–655. [PubMed: 9443060]
44. Witter MP, Griffioen AW, Jorritsma-Byham B, Krijnen JL. Entorhinal projections to the hippocampal CA1 region in the rat: an underestimated pathway. Neurosci Lett. 1988; 85:193–198. [PubMed: 3374835]
45. Tamamaki N. Organization of the entorhinal projection to the rat dentate gyrus revealed by Dil anterograde labeling. Experimental brain research Experimentelle Hirnforschung Experimentation cerebrale. 1997; 116:250–258. [PubMed: 9348124]
46. Steward O, Scoville SA. Cells of origin of entorhinal cortical afferents to the hippocampus and fascia dentata of the rat. The Journal of Comparative Neurology. 1976; 169:347–370. [PubMed: 972204]
47. Tamamaki N, Nojyo Y. Preservation of topography in the connections between the subiculum, field CA1, and the entorhinal cortex in rats. Journal of Comparative Neurology. 1995; 353:379–390. [PubMed: 7538515]
48. Naber PA, Lopes da Silva FH, Witter MP. Reciprocal connections between the entorhinal cortex and hippocampal fields CA1 and the subiculum are in register with the projections from CA1 to the subiculum. Hippocampus. 2001; 11:99–104. [PubMed: 11345131]
49. Honda Y, Sasaki H, Umitsu Y, Ishizuka N. Zonal distribution of perforant path cells in layer III of the entorhinal area projecting to CA1 and subiculum in the rat. Neurosci Res. 2012; 74:200–209. [PubMed: 23131426]
50. Naber PA, Caballero-Bleda M, Jorritsma-Byham B, Witter MP. Parallel input to the hippocampal memory system through peri- and postrhinal cortices. Neuroreport. 1997; 8:2617–2621. [PubMed: 9261838]
51. Naber PA, Witter MP, Lopez da Silva FH. Perirhinal cortex input to the hippocampus in the rat: evidence for parallel pathways, both direct and indirect. A combined physiological and anatomical study. Eur J Neurosci. 1999; 11:4119–4133.
52. Dolorfo CL, Amaral DG. Entorhinal cortex of the rat: organization of intrinsic connections. Journal of Comparative Neurology. 1998; 398:49–82. [PubMed: 9703027]
53. Witter MP, Naber PA, Lopes da Silva F. Perirhinal cortex does not project to the dentate gyrus. Hippocampus. 1999; 9:605–606. [PubMed: 10560931]
54. Naber PA, Witter MP, Lopes da Silva FH. Evidence for a direct projection from the postrhinal cortex to the subiculum in the rat. Hippocampus. 2001; 11:105–117. [PubMed: 11345118]
55. Agster KL, Burwell RD. Cortical efferents of the perirhinal, postrhinal, and entorhinal cortices of the rat. Hippocampus. 2009; 19:1159–1186. [PubMed: 19360714]
56. Burwell RD, Amaral DG. Cortical afferents of the perirhinal, postrhinal, and entorhinal cortices. J Comp Neurol. 1998; 398:179–205. [PubMed: 9700566]
57. Amaral DG, Price JL. An air pressure system for the injection of tracer substances into the brain. J Neurosci Methods. 1983; 9:35–43. [PubMed: 6415347]
58. Burwell RD. Borders and cytoarchitecture of the perirhinal and postrhinal cortices in the rat. Journal of Comparative Neurology. 2001; 437:17–41. [PubMed: 11477594]
59. Gerfen CR, Sawchenko PE. An anterograde neuroanatomical tracing method that shows the detailed morphology of neurons, their axons and terminals: immunohistochemical localization of

NIH-PA Author Manuscript

NIH-PA Author Manuscript

NIH-PA Author Manuscript

an axonally transported plant lectin, *Phaseolus vulgaris*-Leucoagglutinin (PHA-L). Brain Res. 1984; 290:219–238. [PubMed: 6198041]

60. Lewis DA, Campbell MJ, Morrison JH. An immunohistochemical characterization of somatostatin-28 and somatostatin-281-12 in monkey prefrontal cortex. The Journal of Comparative Neurology. 1986; 248:1–18. [PubMed: 2873154]
61. Dobo E, Takacs VT, Gulyas AI, Nyiri G, Mihaly A, Freund TF. New silver-gold intensification method of diaminobenzidine for double-labeling immunoelectron microscopy. J Histochem Cytochem. 2011; 59:258–269. [PubMed: 21378280]
62. Swanson, LW. Brain Maps: Structure of the Rat Brain. 2 ed.. Amsterdam: Elsevier; 1998.
63. Furtak SC, Wei SM, Agster KL, Burwell RD. Functional neuroanatomy of the parahippocampal region in the rat: the perirhinal and postrhinal cortices. Hippocampus. 2007; 17:709–722. [PubMed: 17604355]
64. Kerr KM, Agster KL, Furtak SC, Burwell RD. Functional neuroanatomy of the parahippocampal region: the lateral and medial entorhinal areas. Hippocampus. 2007; 17:697–708. [PubMed: 17607757]
65. Blackstad TW. Commissural connections of the hippocampal region in the rat, with special reference to their mode of termination. The Journal of Comparative Neurology. 1956; 105:417–537. [PubMed: 13385382]
66. Krieg WJ. Connections of the cerebral cortex; the albino rat; structure of the cortical areas. The Journal of Comparative Neurology. 1946; 84:277–323. [PubMed: 20991808]
67. Krieg WJ. Connections of the cerebral cortex; the albino rat; topography of the cortical areas. The Journal of Comparative Neurology. 1946; 84:221–275. [PubMed: 20982805]
68. Witter M, Naber PA, van Haeften T, Machielsen WC, Rombouts SA, Barkhof F, Scheltens P, Lopes da Silva FH. Cortico-hippocampal communication by way of parallel parahippocampal-subicular pathways. Hippocampus. 2000; 10:398–410. [PubMed: 10985279]
69. Van Groen T, Wyss JM. The postsubicular cortex in the rat: characterization of the fourth region of the subicular cortex and its connections. Brain Res. 1990; 529:165–177. [PubMed: 1704281]
70. Witter MP, Ostendorf RH, Groenewegen HJ. Heterogeneity in the Dorsal Subiculum of the Rat. Distinct Neuronal Zones Project to Different Cortical and Subcortical Targets. Eur J Neurosci. 1990; 2:718–725. [PubMed: 12106290]
71. Burwell RD, Amaral DG. Perirhinal and postrhinal cortices of the rat: interconnectivity and connections with the entorhinal cortex. Journal of Comparative Neurology. 1998; 391:293–321. [PubMed: 9492202]
72. Burwell RD, Amaral DG. Perirhinal and postrhinal cortices of the rat: Interconnectivity and connections with the entorhinal cortex. J Comp Neurol. 1998; 391:293–321. [PubMed: 9492202]
73. Burwell RD, Witter MP, Amaral DG. Perirhinal and postrhinal cortices of the rat: a review of the neuroanatomical literature and comparison with findings from the monkey brain. Hippocampus. 1995; 5:390–408. [PubMed: 8773253]
74. Witter MP, Naber PA, van Haeften T, Machielsen WC, Rombouts SA, Barkhof F, et al. Cortico-hippocampal communication by way of parallel parahippocampal-subicular pathways. Hippocampus. 2000; 10:398–410. [PubMed: 10985279]
75. Naber P, Caballero-Bleda M, Jorritsma-Byham B, Witter MP. Parallel input to the hippocampal memory system through peri- and postrhinal cortices. Neuroreport. 1997; 8:2617–2621. [PubMed: 9261838]
76. Naber P, Witter MP, Lopes da Silva FH. Evidence for a direct projection from the postrhinal cortex to the subiculum in the rat. Hippocampus. 2001; 11:105–117. [PubMed: 11345118]
77. Majak K, Pitkanen A. Projections from the periamygdaloid cortex to the amygdaloid complex, the hippocampal formation, and the parahippocampal region: a PHA-L study in the rat. Hippocampus. 2003; 13:922–942. [PubMed: 14750655]
78. Pikkarainen M, Pitkanen A. Projections from the lateral, basal and accessory basal nuclei of the amygdala to the perirhinal and postrhinal cortices in rat. Cereb Cortex. 2001; 11:1064–1082. [PubMed: 11590116]
79. van Strien NM, Cappaert NL, Witter MP. The anatomy of memory: an interactive overview of the parahippocampal-hippocampal network. Nature reviews Neuroscience. 2009; 10:272–282.

NIH-PA Author Manuscript

NIH-PA Author Manuscript

NIH-PA Author Manuscript

80. Sugar J, Witter MP, van Strien NM, Cappaert NL. The retrosplenial cortex: intrinsic connectivity and connections with the (para)hippocampal region in the rat. An interactive connectome. Front Neuroinform. 2011; 5:7.
81. Hjorth-Simonsen A. Hippocampal efferents to the ipsilateral entorhinal area: an experimental study in the rat. The Journal of Comparative Neurology. 1971; 142:417–437. [PubMed: 4106861]
82. Beckstead RM. Afferent connections of the entorhinal area in the rat as demonstrated by retrograde cell-labeling with horseradish peroxidase. Brain Research. 1978; 152:249–264. [PubMed: 679029]
83. Swanson LW, Cowan WM. An autoradiographic study of the organization of the efferent connections of the hippocampal formation in the rat. The Journal of Comparative Neurology. 1977; 172:49–84. [PubMed: 65364]
84. Swanson LW, Wyss JM, Cowan WM. An autoradiographic study of the organization of intrahippocampal association pathways in the rat. The Journal of Comparative Neurology. 1978; 181:681–715. [PubMed: 690280]
85. Swanson LW, Kohler C. Anatomical evidence for direct projections from the entorhinal area to the entire cortical mantle in the rat. The Journal of neuroscience : the official journal of the Society for Neuroscience. 1986; 6:3010–3023. [PubMed: 3020190]
86. Wyss JM. An autoradiographic study of the efferent connections of the entorhinal cortex in the rat. The Journal of Comparative Neurology. 1981; 199:495–512. [PubMed: 6168668]
87. Kohler C, Shipley MT, Srebro B, Harkmark W. Some retrohippocampal afferents to the entorhinal cortex. Cells of origin as studied by the HRP method in the rat and mouse. Neurosci Lett. 1978; 10:115–120. [PubMed: 19605266]
88. Kohler C. Intrinsic connections of the retrohippocampal region in the rat brain. II. The medial entorhinal area. Journal of Comparative Neurology. 1986; 246:149–169. [PubMed: 3958250]
89. Kohler C. Intrinsic connections of the retrohippocampal region in the rat brain: III. The lateral entorhinal area. The Journal of Comparative Neurology. 1988; 271:208–228. [PubMed: 3379162]
90. Caballero-Bleda M, Witter MP. Regional and laminar organization of projections from the presubiculum and parasubiculum to the entorhinal cortex: an anterograde tracing study in the rat. The Journal of Comparative Neurology. 1993; 328:115–129. [PubMed: 8429124]
91. Honda Y, Ishizuka N. Organization of connectivity of the rat presubiculum: I. Efferent projections to the medial entorhinal cortex. Journal of Comparative Neurology. 2004; 473:463–484. [PubMed: 15116384]
92. Wouterlood FG, Van Haeften T, Eijkhoudt M, Baks-Te-Bulte L, Goede PH, Witter MP. Input from the presubiculum to dendrites of layer-V neurons of the medial entorhinal cortex of the rat. Brain Res. 2004; 1013:1–12. [PubMed: 15196963]
93. Boccara CN, Sargolini F, Thoresen VH, Solstad T, Witter MP, Moser EI, et al. Grid cells in pre- and parasubiculum. Nature neuroscience. 2010; 13:987–994.
94. Taube JS. Place cells recorded in the parasubiculum of freely moving rats. Hippocampus. 1995; 5:569–583. [PubMed: 8646283]
95. Yoder RM, Clark BJ, Taube JS. Origins of landmark encoding in the brain. Trends Neurosci. 2011; 34:561–571. [PubMed: 21982585]
96. Bett D, Stevenson CH, Shires KL, Smith MT, Martin SJ, Dudchenko PA, et al. The postsubiculum and spatial learning: the role of postsubicular synaptic activity and synaptic plasticity in hippocampal place cell, object, and object-location memory. The Journal of neuroscience : the official journal of the Society for Neuroscience. 2013; 33:6928–6943. [PubMed: 23595751]
97. van Groen T, Wyss JM. The connections of presubiculum and parasubiculum in the rat. Brain Research. 1990; 518:227–243. [PubMed: 1697208]
98. Furtak SC, Ahmed OJ, Burwell RD. Single neuron activity and theta modulation in postrhinal cortex during visual object discrimination. Neuron. 2012; 76:976–988. [PubMed: 23217745]
99. Kahn I, Andrews-Hanna JR, Vincent JL, Snyder AZ, Buckner RL. Distinct cortical anatomy linked to subregions of the medial temporal lobe revealed by intrinsic functional connectivity. Journal of neurophysiology. 2008; 100:129–139. [PubMed: 18385483]
100. Vincent JL, Kahn I, Van Essen DC, Buckner RL. Functional connectivity of the macaque posterior parahippocampal cortex. Journal of neurophysiology. 2010; 103:793–800. [PubMed: 19955295]

101. Suzuki WA, Amaral DG. Perirhinal and parahippocampal cortices of the macaque monkey: cortical afferents. The Journal of Comparative Neurology. 1994; 350:497–533. [PubMed: 7890828]

NIH-PA Author Manuscript

NIH-PA Author Manuscript

NIH-PA Author Manuscript

NIH-PA Author Manuscript

NIH-PA Author Manuscript

NIH-PA Author Manuscript

Highlights

- We examined the hippocampal connections of three parahippocampal structures.
- Perirhinal projections are stronger to the ventral hippocampus.
- Postrhinal projections are stronger to the dorsal hippocampus.
- Entorhinal connections differ across dentate-gyrus projecting bands.

NIH-PA Author Manuscript
NIH-PA Author Manuscript
NIH-PA Author Manuscript

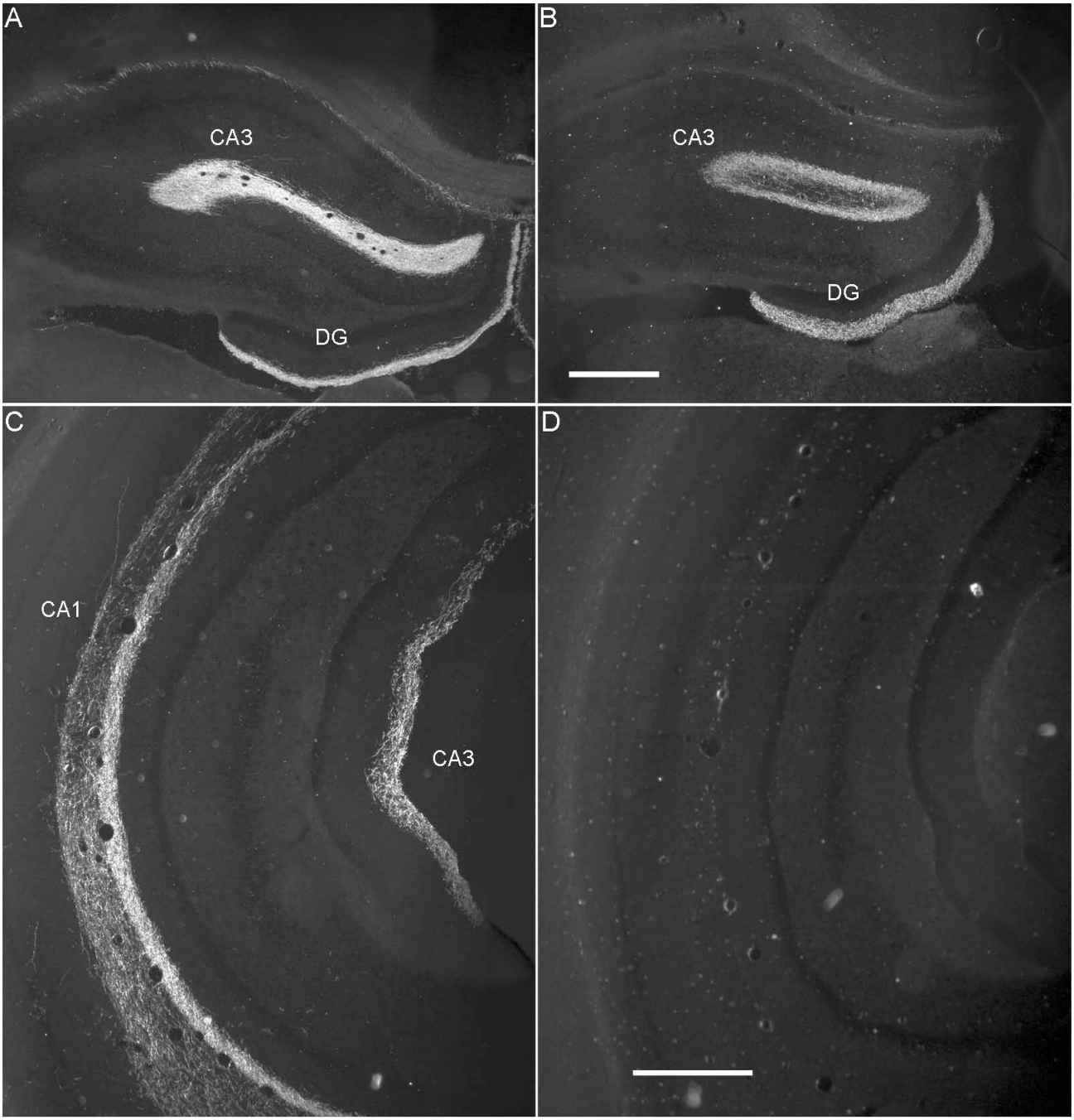

Figure 1.
Hippocampal and parahippocampal target regions. Panels A and B show the locations of the dentate gyrus (green), hippocampal fields CA3 (blue), CA2 (light purple), CA1 (red), and subiculum (yellow). Panels C and D also the dentate gyrus and parahippocampal region structures, the presubiculum (light orange) and parasubiculum (dark orange) are shaded with hatch marks. PER, POR, LEA, and MEA are shown in grey.

NIH-PA Author Manuscript

NIH-PA Author Manuscript

NIH-PA Author Manuscript

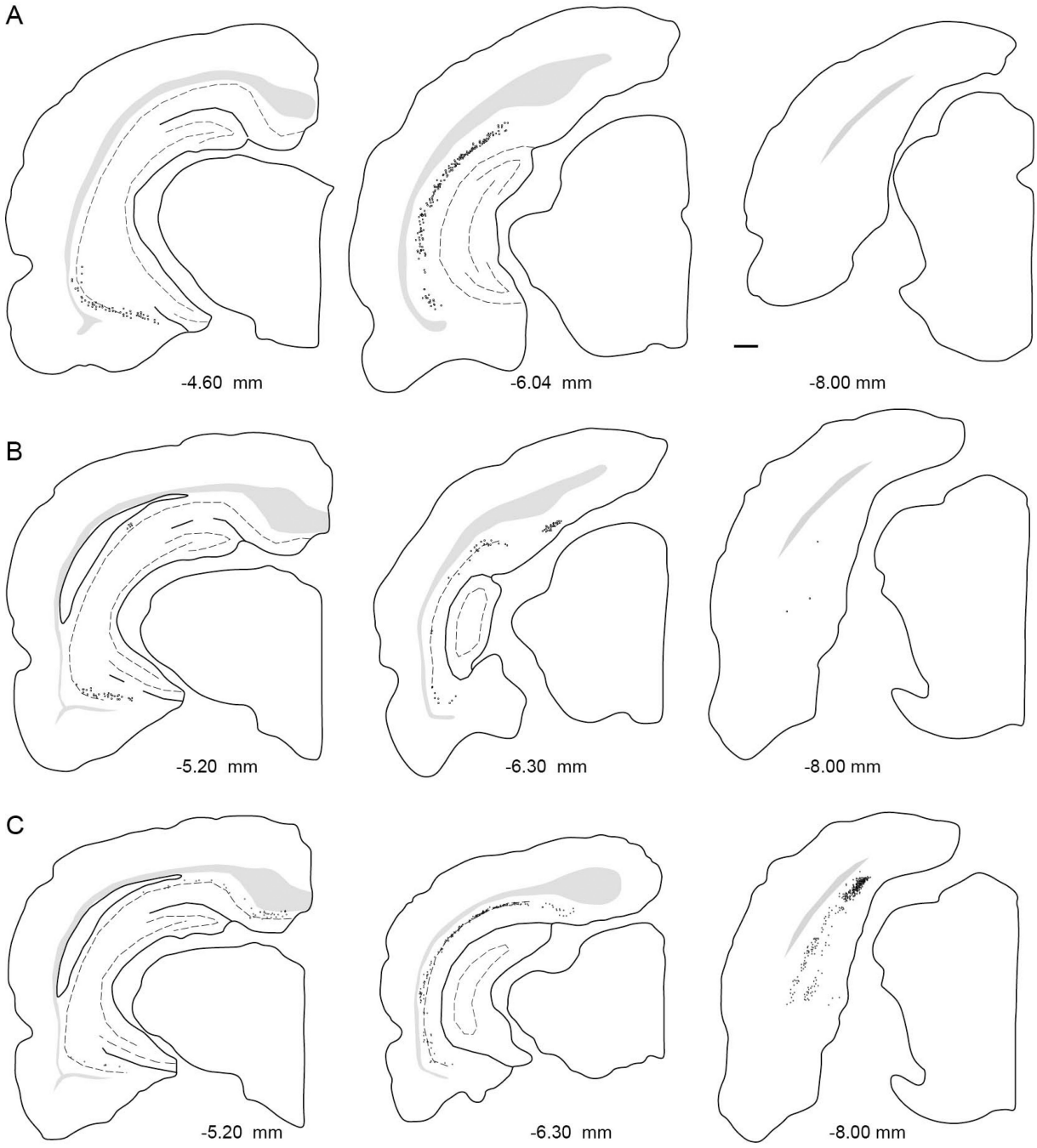

Figure 2.

Location of the retrograde and anterograde tracer injection sites to the perirhinal, postrhinal, and entorhinal cortices. Injection sites are represented on two-dimensional unfolded maps of the cortical regions. Dark grey tones indicate injection sites to deep layers of cortex, medium grey tones indicate injection sites that span deep and superficial layers of cortex, and light grey tones are indicative of injection sites to superficial cortical layers. A. Retrograde tracer injection sites. B. Anterograde tracer injection sites. Dashed line in all panels represents the rhinal sulcus. Adapted from Burwell and Amaral, 1998. Scale bar = 1mm.

NIH-PA Author Manuscript
NIH-PA Author Manuscript
NIH-PA Author Manuscript

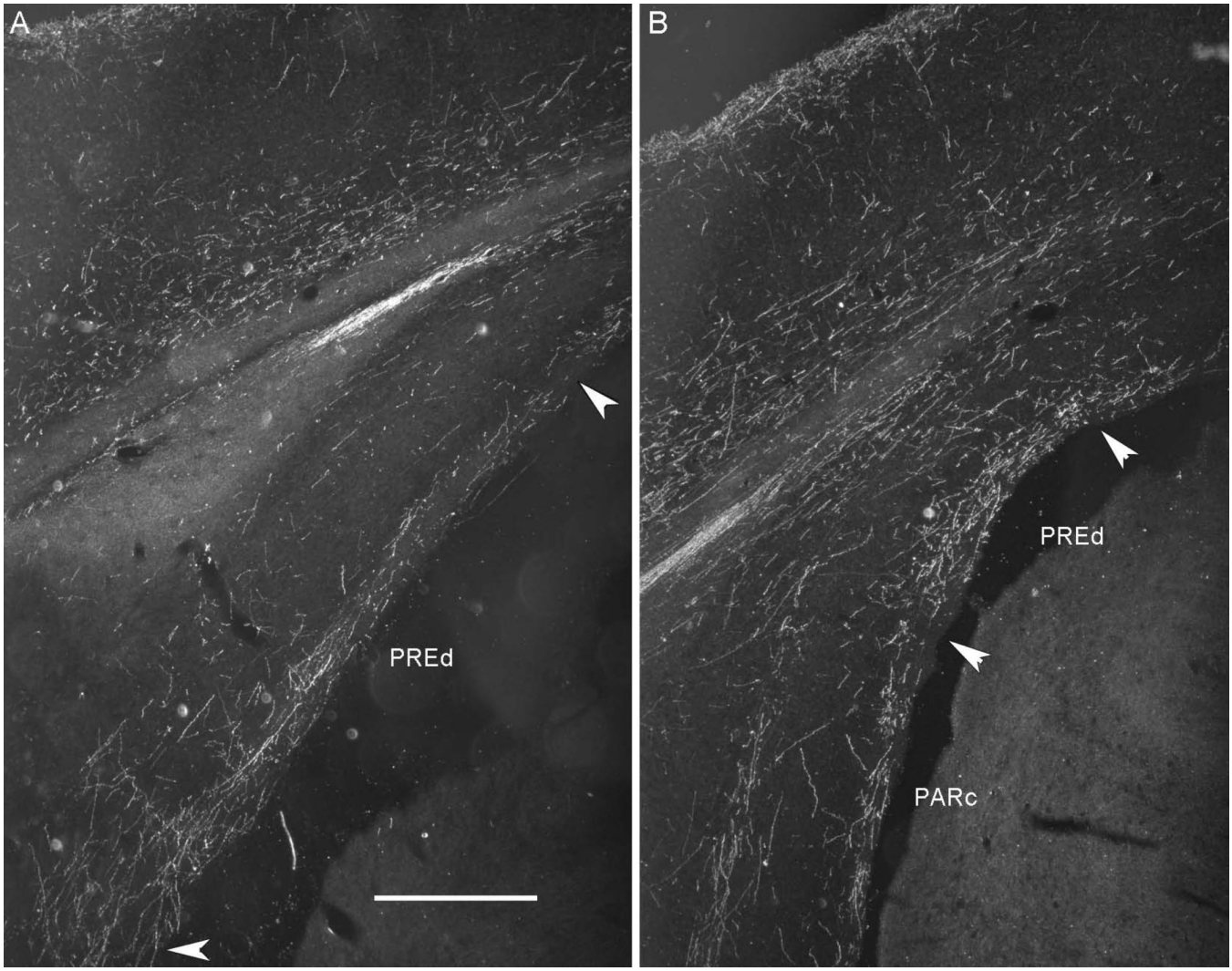

Figure 3.
Examples of anterograde and retrograde tracer injection sites. Shown are a Pha-L site in POR, 40P at −8.1 mm relative to β (A), a biotinylated dextrane site in the LEA, 61B at −6.5 mm relative to β (B), a diamidino yellow site in PER area 36, 98DY at −5.1 mm relative to β (C), and a diamidino yellow site in the MEA, 124DY, at −7.8 mm relative to β (D). Scale bar: 500 microns.

NIH-PA Author Manuscript
NIH-PA Author Manuscript
NIH-PA Author Manuscript

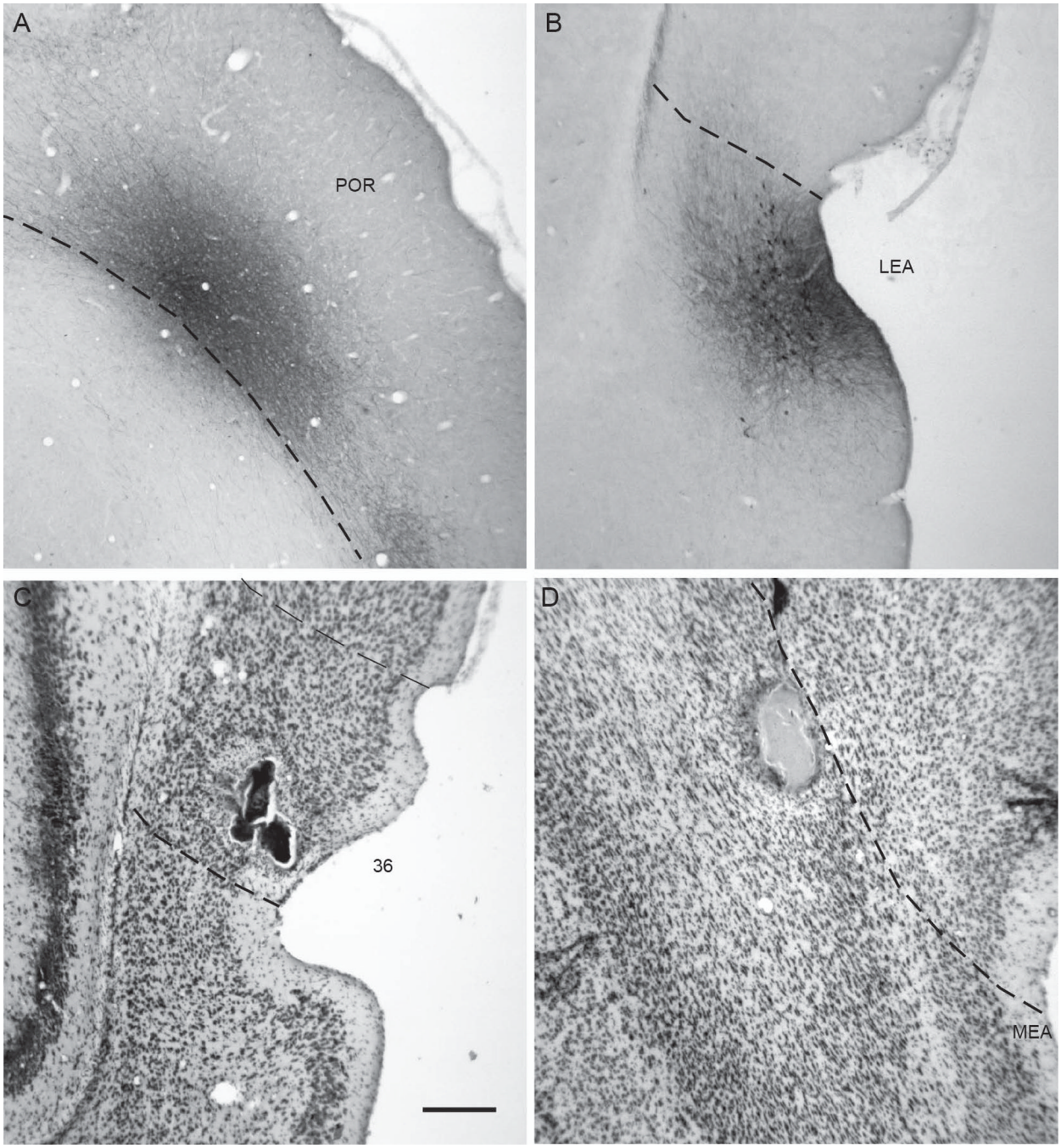

Figure 4.
Darkfield photomicrographs showing the distribution of fiber labeling in the dorsal presubiculum following an antergrade tracer injection to the postrhinal cortex (POR, Case 40P, −8.1 mm relative to β). The strongest projection from the POR terminated in the dorsal presubiculum (PREd). A. Fiber labeling in PREd at −7.0 mm from bregma. B. Fiber labeling in PREd at −8.0 mm from bregma. Scale bar: 500 microns.

NIH-PA Author Manuscript

NIH-PA Author Manuscript

NIH-PA Author Manuscript

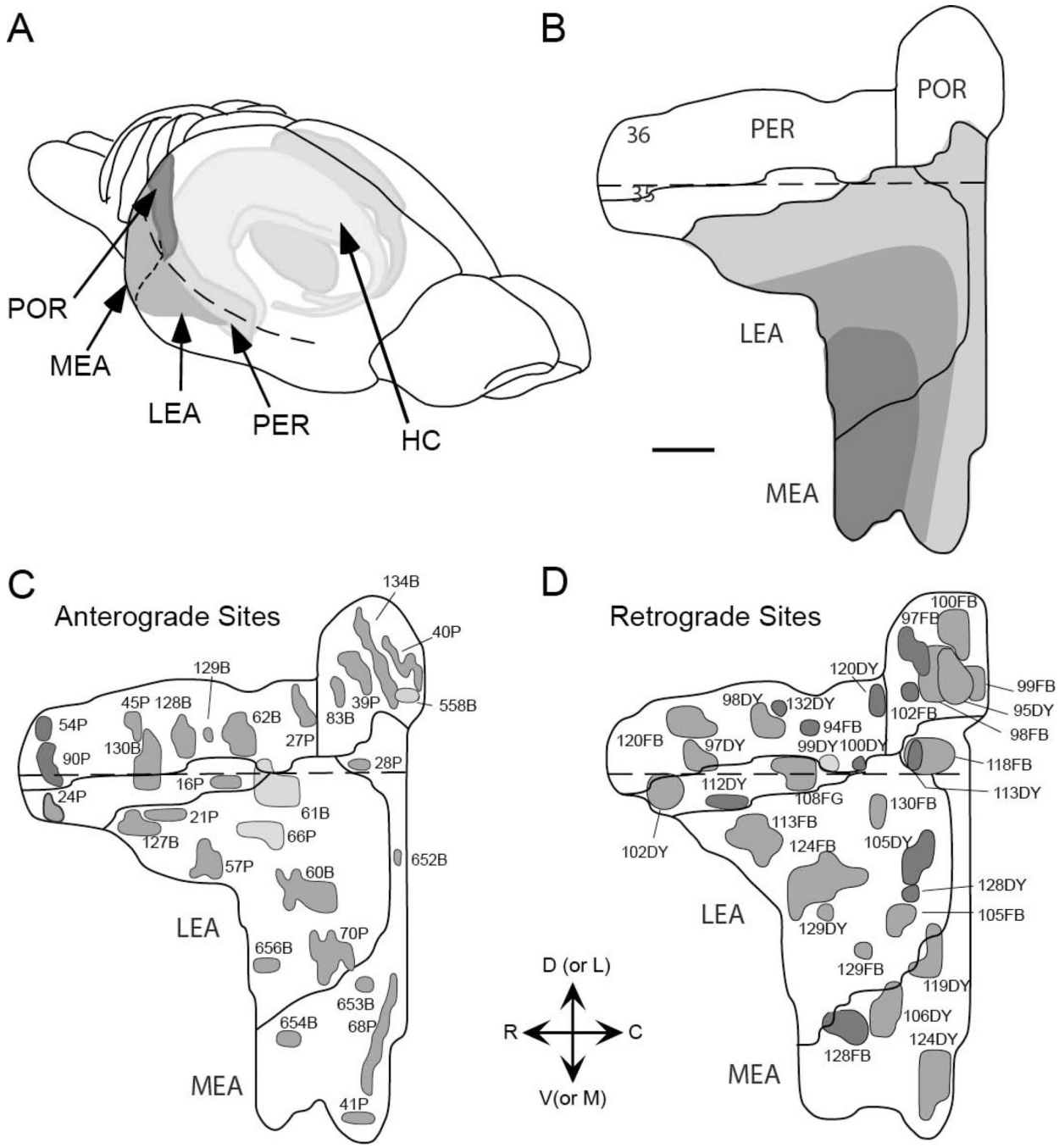

Figure 5.

Distribution of labeled cells arising from injection sites in PER area 35, PER area 36, and the POR. A. Computer generated plots showing the distribution of retrogradely-labeled cells in the hippocampus and subiculum, following tracer injection perirhinal area 35 (Case 112DY, −3.7 mm relative to β). B. Computer generated plots showing the distribution of retrogradely-labeled cells in the hippocampus and subiculum, following tracer injection in perirhinal area 36 (Case 98DY, −5.1 mm relative to β). C. Computer generated plots showing the distribution of retrogradely-labeled cells in the hippocampus and subiculum, following tracer injection postrhinal cortex (Case 98FB, −7.8 mm relative to β).

NIH-PA Author Manuscript
NIH-PA Author Manuscript
NIH-PA Author Manuscript

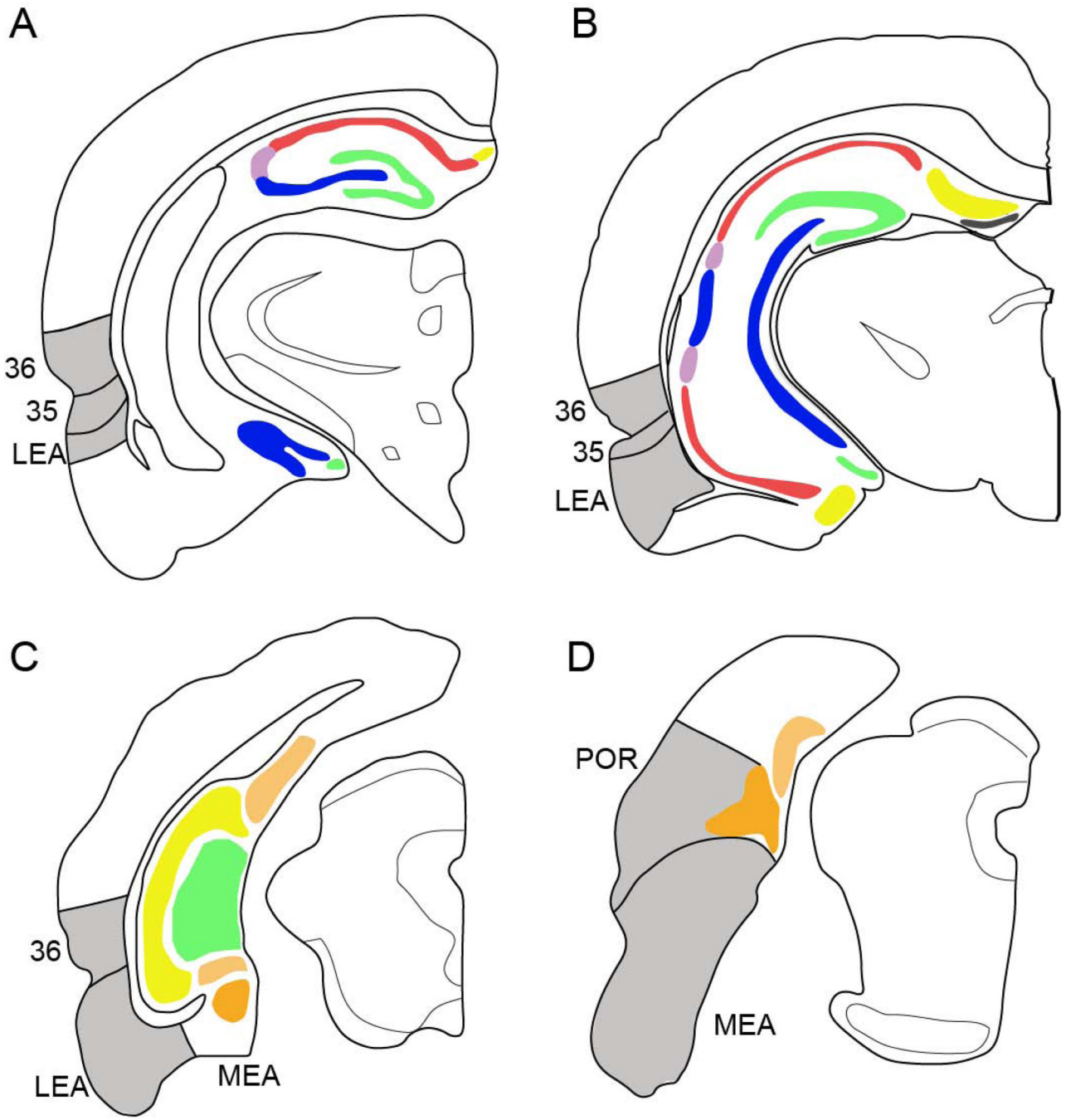

Figure 6.

Darkfield photomicrographs showing the distribution of labeled fibers in the dorsal and ventral hippocampus following tracer injections to the lateral entorhinal area. A and C. Fiber labeling in dorsal (A) and ventral (C) hippocampal regions as a result of anterograde tracer injection to the lateral band of the LEA (Case 61B). B and D. Fiber labeling in dorsal (B) and ventral (D) hippocampal regions as a result of anterograde tracer injection to the lateral band of the MEA (Case 41P). Both injection sites were located in the lateral band, but only the LEA injection results in fiber labeling in ventral hippocampus. Scale bar: 500 microns.

NIH-PA Author Manuscript
NIH-PA Author Manuscript
NIH-PA Author Manuscript

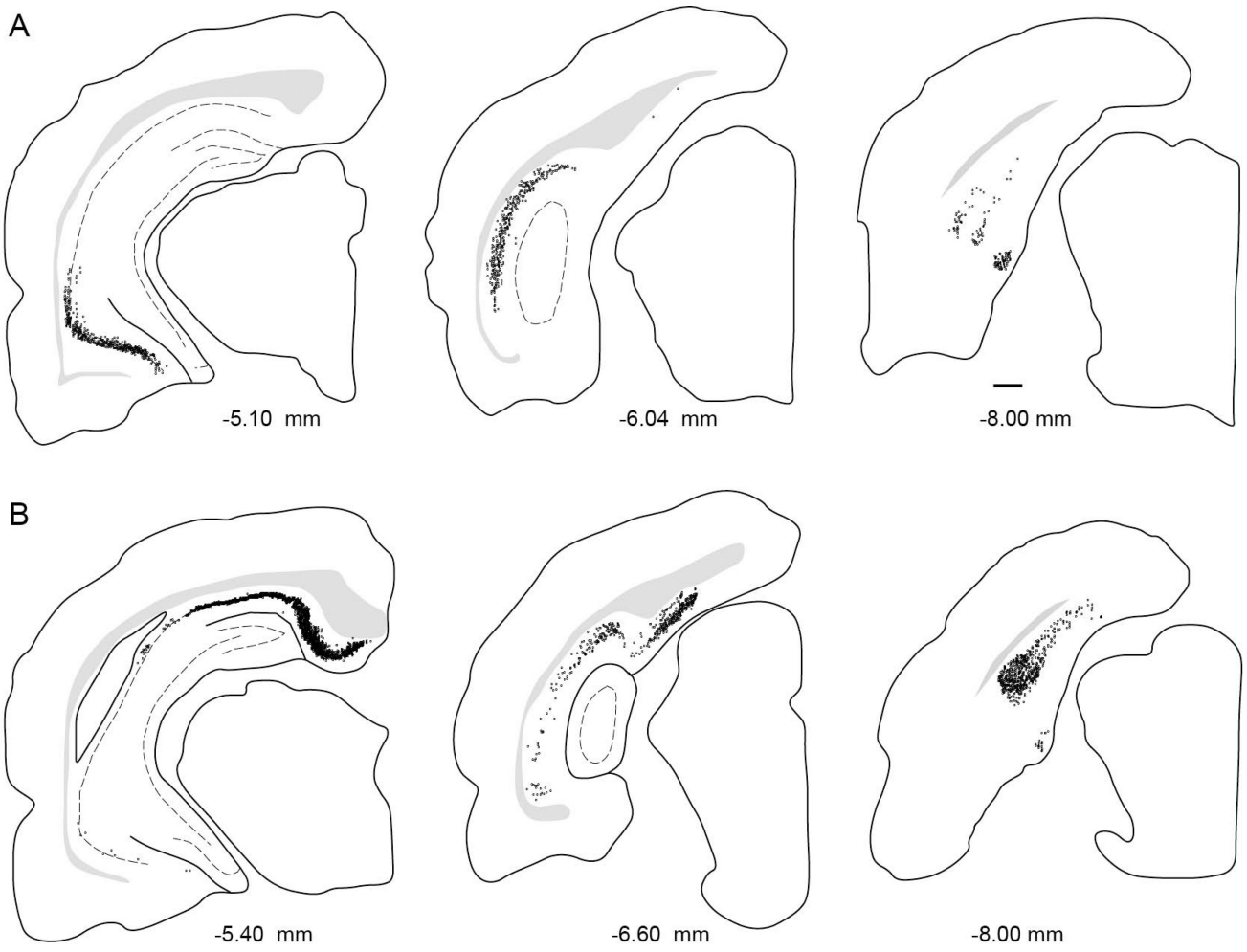

Figure 7.

Distribution of labeled cells arising from injection sites located in the LEA and MEA. Computer generated plots showing the distribution of retrogradely-labeled cells in the hippocampal and parahippocampal areas, following tracer injections. A. Computer-generated plots showing the distribution retrogradely-labeled cells in hippocampal structures arising from an LEA injection site (Case 124FB, −5.4 mm relative to β). B. L Computer-generated plots showing the distribution retrogradely-labeled cells in hippocampal structures arising from an MEA injection site (Case 113DY, −7.6 mm relative to β).

NIH-PA Author Manuscript

NIH-PA Author Manuscript

NIH-PA Author Manuscript

Table 1

Anterograde Tracer Injection Sites

Location	Experiment	Layer	Size (μm)
Perirhinal Area 36			
Rostral area 36	45P	III–VI	400
Rostral area 36	54P	V–VI	400
Midrostrocaudal area 36	62B	II–V	400
Midrostrocaudal area 36	90P	V–VI	300
Midrostrocaudal area 36	128B	II–VI	400
Caudal area 36	27P	II–VI	300
Ventral area 36	129B	II–V	300
Ventral area 36	[1]130B	III–VI	400
Perirhinal Area 35			
Rostral area 35	24P	III–VI	300
Caudal area 35	16B	II–V	400
Postrhinal			
Rostral	39P	I–VI	400
Rostrodorsal	83B	IV–VI	500
Dorsal	134B	I–VI	500
Caudal	40P	III–VI	500
Caudal	558B	I–III	300
Entorhinal LEA			
Rostral LEA, L	21P	III–V	300
Rostral LEA, L	57P	II–VI	400
Rostral LEA, L	[2]61B	I–III	400
Rostral LEA, L	127B	III–VI	500
Midrostrocaudal LEA, L	66P	II–III	300
Midrostrocaudal LEA, I	60B	II–V	700
Caudomedial LEA, I	70P	II–IV	400
Caudal LEA, M	656B	II–V	500
Entorhinal MEA			
Lateral MEA, L	28P	III–VI	300
Caudal MEA, L	652B	II–VI	300
Medial MEA, L	68P	II–VI	500
Medial MEA, L	41P	II–VI	200
Caudomedial MEA, L/I	[3]653B	II–VI	300
Medial MEA, M	654B	II–VI	400

Anterograde injections sites are suffixed with a P or a B for PHA-L and BDA, respectively.

[1] Experiment 130B encroached slightly on area 35.

[2] Experiment 61B encroached slightly on superficial layers of area 36.

[3]Experiment 653B was located on the border between the lateral and intermediate bands.

Abbreviations: L, lateral dentate gyrus-projecting band; I, intermediate band; M, medial band.

NIH-PA Author Manuscript

NIH-PA Author Manuscript

NIH-PA Author Manuscript

NIH-PA Author Manuscript

NIH-PA Author Manuscript

NIH-PA Author Manuscript

Table 2

Retrograde Tracer Injection Sites

Location	Experiment	Layer	Size (μm)
Perirhinal Area 36			
Rostrodorsal area 36	120 FB	III–V	700
Rostroventral area 36	97 DY	III–V	500
Midrostrocaudal area 36	98 DY	I–V	300
Midrostrocaudal area 36	132 DY	V	200
Midrostrocaudal area 36	94 FB	V	400
Caudoventral area 36	*1*99 DY	II–III	300
Caudoventral area 36	100 DY	V	300
Caudodorsal area 36	120 DY	V	300
Perirhinal Area 35			
Rostral area 35	102 DY	I–V	400
Rostroventral area 35	132 FB	V–VI	300
Ventral area 35	112 DY	V	400
Caudal area 35	*2*108 FG	I–VI	300
Postrhinal			
Rostral POR	97 FB	V	400
Rostroventral POR	102 FB	V	200
Middle POR	98 FB	I–VI	600
Caudodorsal POR	100 FB	I–V	500
Caudal POR	95 DY	III–VI	400
Caudal POR	99 FB	I–V	500
Entorhinal LEA			
Rostrolateral LEA, L	113 FB	I–V	600
Caudolateral LEA, L	130 FB	V–VI	400
Rostral LEA, I	124 FB	I–VI	800
Caudal LEA, I	105 DY	V	400
Caudal LEA, I	128 DY	V	300
Caudomedial LEA, I	105 FB	III–VI	400
Medial LEA, I	129 FB	V–VI	300
Rostral LEA, M	129 DY	III–V	300
Entorhinal MEA			
Lateral MEA, L	113 DY	V	300
Lateral MEA, L	118 FB	III–VI	600
Caudomedial MEA, L	124 DY	I–V	600
Caudal MEA, I	119 DY	I–V	400
Medial MEA, M	106 DY	II–VI	500
Medial MEA, M	128 FB	V	300

Retrograde injections sites are suffixed with a FB, DY, or FG for Fast Blue, Diamidino Yellow, or Fluorogold, respectively.

[1]For experiment 99DY, the injection site was excluded from analyses as there was negligible labeling due to superficial location of site.

[2]Experiment 108 FG encroached slightly on LEA. Other abbreviations: L, lateral dentate gyrus-projecting band; I, intermediate band; M, medial band.

NIH-PA Author Manuscript
NIH-PA Author Manuscript
NIH-PA Author Manuscript

NIH-PA Author Manuscript
NIH-PA Author Manuscript
NIH-PA Author Manuscript

Table 3

Output to PER, POR and ER: Density of anterogradely-labeled fibers

	Perirhinal		Postrhinal	Entorhinal	
Efferents	**Area 35**	**Area 36**		**LEA**	**MEA**
DORSAL HC					
DGd	-	-	+	+++++	++++++
CA3d	-	-	+	++	+++
CA2d	-	+	+	++++	++++
CA1d	-	+	++	+++++	++++++
SUBd	+	+	+++	++++	+++++
VENTRAL HC					
DGv	-	-	-	++++	++++
CA3v	-	+	+	+++	+++
CA2v	-	+	-	+++	++++
CA1v	+	++	+	+++++	++++
SUBv	++	++	++	++++	++++
PARAHC					
PREd	+	++	++++++	+++++	++++
PREv	-	+	+++	++++	+++
PARr	+	++	+++	++++	+++
PARc	-	++	+++++	+++	++++++

Data are average density of labeling across the efferent regions listed in the left column. Only 2 cases are available for area 35, but the cases exhibited good labeling, were distributed along the rostrocaudal axis, and involved both deep and superficial layers. See text for details of how fiber density was quantified. Legend: -, no observed label; +, negligible; ++, very sparse; +++, sparse; ++++, moderately dense; +++++, dense; ++++++, very dense.

NIH-PA Author Manuscript
NIH-PA Author Manuscript
NIH-PA Author Manuscript

Table 4

Input to PER, POR and ER: Density of retrogradely-labeled cells

	Perirhinal		Postrhinal	Entorhinal	
Afferents	**Area 35**	**Area 36**		**LEA**	**MEA**
DORSAL HC					
DGd	0±0	0±0	0±0	1±1	12±8
CA3d	10±10*	4±2	2±2*	51±39	51±35
CA2d	101±101*	26±26*	31±17	133±52	674±358
CA1d	339±184	115±94	773±408	678±261	3035±2326
SUBd	1242±671	138±94	1200±446	1146±240	2065±1269
VENTRAL HC					
DGv	0±0	1±1	0±0	14±6	23±11
CA3v	37±37*	9±7	0±0	346±297	743±508
CA2v	1246±1246*	98±93	29±18	6459±417	3355±3070
CA1v	1525±1045	1035±298	527±182	5720±771	2028±1187
SUBv	1418±1084	553±129	470±115	3745±265	3311±1661
PARAHC					
PREd	178±130	43±34	1112±455	465±305	7898±3232
PREv	521±521	248±245	336±240	1751±1137	3552±1728
PARr	1059±932	203±93	271±126	2225±1212	2846±1206
PARc	494±376	564±205	8171±2082	1003±404	7839±3968

Data are mean density±standard error of retrogradely-labeled cells per cubic millimeter for each structure. Density was calculated for each case for each of the 14 hippocampal and parahippocampal afferent areas using normalized data. See text for details about normalization.

*Cells in this area were only observed in a single case: 108FG for area 35, 100DY for area 36, and 97FB for POR. Sites 108FG and 100DY were located close to the entorhinal border, but 97FB was not. Note that densities are given in cells/mm^3, and that smaller densities may represent such a small number of cells as to be considered negligible.

NIH-PA Author Manuscript
NIH-PA Author Manuscript
NIH-PA Author Manuscript

Behav Brain Res. Author manuscript; available in PMC 2014 October 01.

Table 5

Input to PER, POR and ER: Percentage of total retrogradely-labeled cells

	Perirhinal		Postrhinal	Entorhinal	
Afferents	**Area 35**	**Area 36**		**LEA**	**MEA**
DORSAL HC					
DGd	0.00±0.00	0.00±0.00	0.00±0.00	0.02±0.01	0.15±0.11
CA3d	0.20±0.20*	0.04±0.04*	0.02±0.02*	0.38±0.22	0.36±0.22
CA2d	0.45±0.45*	0.03±0.03*	0.10±0.05	0.21±0.09	0.62±0.35
CA1d	17.24±7.19	6.40±4.30	16.26±8.64	13.68±5.21	22.79±15.24
SUBd	12.78±6.28	2.64±1.15	5.78±2.23	6.22±2.16	4.08±2.18
VENTRAL HC					
DGv	0.00±0.00	0.00±0.00	0.00±0.00	0.08±0.02	0.15±0.09
CA3v	0.73±0.74*	0.00±0.00	0.00±0.00	1.30±0.89	4.29±2.76
CA2v	2.82±2.85*	0.35±0.21	0.07±0.06	1.94±0.76	1.27±1.04
CA1v	38.87±23.73	57.10±5.20	6.30±2.05	42.21±7.05	10.92±5.41
SUBv	13.73±8.85	19.14±4.76	3.14±0.83	18.01±5.57	9.29±3.82
PARAHC					
PREd	1.47±0.89	3.41±1.25	33.08±6.80	3.48±1.54	19.76±7.83
PREv	2.89±2.92	0.11±0.08	0.73±0.44	4.15±2.11	3.96±1.71
PARr	4.70±3.86	1.49±0.57	0.57±0.18	5.06±2.37	2.36±0.94
PARc	4.10±3.11	9.27±3.96	33.97±6.03	3.26±1.24	20.00±15.02
TOTAL PCT	100.00	100.00	100.00	100.00	100.00
TOTAL CELLS	11088±6662	8855±3613	15854±3737	54720±11062	64157±12896

Data are mean percentage ± standard error of input based on total normalized labeled cells arising from retrograde tracer injections. Mean totals of normalized cell counts are shown in bottom row.

*Cells in these areas were observed in a single case, only: 108FG for area 35, 100DY for area 36, and 97FB for POR. Sites 108FG and 100DY were located close to the entorhinal border, but 97FB was not. Note that inputs comprising less than 1% total should be interpreted with caution.

NIH-PA Author Manuscript NIH-PA Author Manuscript NIH-PA Author Manuscript

Table 6

Output from ER DG-projecting bands: Density of anterogradely-labeled fibers

	Lateral Entorhinal Area			Medial Entorhinal Area		
Efferents	**Lateral**	**Intermediate**	**Medial**	**Lateral**	***Intermediate**	**Medial**
DORSAL HC						
DGd	+++++	++++	+	++++++		++
CA3d	++	+++	+++	++++		+++
CA2d	+++	+++++	+++	++++		++
CA1d	+++++	+++	+++	+++++		++
SUBd	+++++	+++	++	+++++		-
VENTRAL HC						
DGv	+++	+++++	+++++	++++		++++++
CA3v	+	++++	+++++	+++		++++++
CA2v	++	++++	+++++	++++		+++++
CA1v	+++++	+++++	++++++	++++		++++++
SUBv	++++	+++++	+++++	++++		++++++
PARAHC						
PREd	+++++	++++	-	++++		++
PREv	++++	+++++	++	++++		++++++
PARr	+++	+++	-	++++++		+++++
PARc	+++	++++	+++++	+++		++++++

Data are average density of terminal fiber labeling across the entorhinal (ER) efferent regions. Density of fiber labeling was averaged for each of the dentate-gyrus (DG) projecting bands of the entorhinal cortex. See text for details of how fiber density was quantified. Only one injection site was located in the LEA medial band and the MEA medial band.

*No injection sties were clearly located in the intermediate band of the MEA. Legend: -, no observed label; +, negligible; ++, very sparse; +++, sparse; ++++, moderately dense; +++++, dense; ++++++, very dense.

NIH-PA Author Manuscript NIH-PA Author Manuscript NIH-PA Author Manuscript

Table 7

Input to ER DG-projecting bands: Density of retrogradely-labeled cells

	Lateral Entorhinal Area			Medial Entorhinal Area		
Afferents	**Lateral**	**Intermediate**	**Medial**	**Lateral**	**Intermediate**	**Medial**
DORSAL HC						
DGd	0	2	0	20	10	2
CA3d	23	7	322	26	4	111
CA2d	66	156	151	971	44	543
CA1d	382	883	247	6044	4	36
SUBd	1328	1074	1140	4039	69	101
VENTRAL HC						
DGv	0	18	27	1	57	38
CA3v	38	54	2424	2	22	2216
CA2v	3158	1665	10104	48	178	9906
CA1v	3657	4249	17199	626	282	5005
SUBv	1538	3113	11320	1327	662	7611
PARAHC						
PREd	1322	160	279	14972	548	963
PREv	1079	485	9431	1787	3704	6125
PARr	1111	1050	10328	1120	3039	5337
PARc	1131	1084	345	13820	4185	695

Data are mean density±standard error of retrogradely-labeled cells per cubic millimeter for each dentate gyrus (DG)-projecting entorhinal (ER) band. Density was calculated for each case for each of the 14 hippocampal and parahippocampal afferent areas using normalized data. See text for details about normalization. Note there was only one injection site in the LEA medial band and in the MEA lateral band. Note that densities are given in cells/mm^3, and that smaller densities may represent such a small number of cells as to be considered negligible.

NIH-PA Author Manuscript NIH-PA Author Manuscript NIH-PA Author Manuscript

Table 8

Input to ER DG-projecting bands: Percentage total retrogradely-labeled cells

	Lateral Entorhinal Area			Medial Entorhinal Area		
Afferents	**Lateral**	**Intermediate**	**Medial**	**Lateral**	**Intermediate**	**Medial**
DORSAL HC						
DGd	0.00	0.02	0.00	0.18	0.69	0.02
CA3d	0.50	0.34	1.29	0.16	0.23	0.92
CA2d	0.15	0.25	0.10	0.67	0.46	0.61
CA1d	11.56	13.59	1.76	33.88	0.46	0.49
SUBd	11.73	4.72	1.94	5.89	1.39	0.38
VENTRAL HC						
DGv	0.00	0.10	0.06	0.00	2.31	0.30
CA3v	0.39	1.62	5.50	0.01	0.92	16.03
CA2v	2.34	1.83	4.63	0.01	0.92	4.65
CA1v	38.13	43.25	50.58	2.39	14.79	33.33
SUBv	15.59	20.05	17.98	2.62	14.79	26.63
PARAHC						
PREd	7.19	0.80	0.35	23.33	5.31	2.05
PREv	4.09	4.56	5.09	0.94	39.05	7.84
PARr	2.68	6.23	10.23	0.96	9.47	5.32
PARc	5.61	2.55	0.49	28.89	9.24	1.48
TOTAL PCT	100	100	100	100	100	100

Data are mean percentage of input based on total normalized labeled cells arising from retrograde tracer injections for each dentate gyrus (DG)-projecting entorhinal (ER) band. See text for details about normalization. Note that inputs comprising less than 1% total should be interpreted with caution.